INVESTIGATING FORMALDEHYDE TO

NITROGEN DIOXIDE RATIOS USING SATELLITE, IN SITU,

AND AIR QUALITY MODELING DATA

by

J. Jerrold M. Acdan

A thesis submitted in partial fulfilment of

the requirements for the degree of

Master of Science

(Atmospheric and Oceanic Sciences)

at the

UNIVERSITY OF WISCONSIN-MADISON

2021

THESIS DECLARATION & APPROVAL

I, J. Jerrold M. Acdan, declare that this thesis entitled 'Investigating Formaldehyde to Nitrogen Dioxide Ratios Using Satellite, In Situ, and Air Quality Modeling Data' and the work presented in it are my own:

J. Jerrold M. Acdan	*J. Jerrold M. Acdan*	08/12/2021
Author	**Signature**	**Date**

I hereby approve and recommend for acceptance this work in partial fulfillment of the requirements for the degree of Master of Science:

Professor R. Bradley Pierce		08/12/2021
Committee Chair	**Signature**	**Date**

Professor Tracey Holloway	*J Holloway*	08/12/2021
Faculty Member	**Signature**	**Date**

Professor Timothy Bertram		08/12/2021
Faculty Member	**Signature**	**Date**

ABSTRACT

Investigating Formaldehyde to Nitrogen Dioxide Ratios Using

Satellite, In Situ, and Air Quality Modeling Data

by J. Jerrold M. Acdan

The use of the formaldehyde (HCHO) to nitrogen dioxide (NO_2) ratio ($HCHO/NO_2$; 'FNR') as an indicator for tropospheric ozone production sensitivity is an active area of research. Early studies in this topic conducted air quality model simulations to determine FNR threshold values for different ozone production regimes and applied them to FNRs calculated from satellite data to assess ozone production sensitivity for various regions across the globe. More recent work determined FNR threshold values through connecting satellite FNRs to in situ ozone data collected by surface monitors. This thesis contributes to the growing body of FNR-related research by utilizing satellite, in situ, and air quality modeling data to evaluate FNRs over the Lake Michigan region while interpreting them using two distinct sets of ozone production regime threshold values from previous studies.

Composites of TROPOspheric Monitoring Instrument (TROPOMI) satellite retrievals of NO_2 and HCHO were created on a monthly basis to reduce the influence of noise in the HCHO retrievals. Based on FNR values, a combined 2018-2019 ozone season composite indicated that in the Lake Michigan region, the Chicago Metropolitan Area is VOC-sensitive, its surroundings and north along the Wisconsin shoreline up to Milwaukee are in the transition zone, and the rest of the region falls within the NO_x-sensitive ozone production regime. Further

analysis showed that FNR values within the domain are greater during ozone exceedance days, which is largely driven by changes in background HCHO concentrations.

When compared to FNRs calculated from U.S. Environmental Protection Agency (EPA) Photochemical Assessment Monitoring Stations (PAMS) surface measurements, the TROPOMI tropospheric column FNRs are larger. To investigate these differences, in situ measurements from the Lake Michigan Ozone Study (LMOS) 2017 field campaign and high-resolution Community Multiscale Air Quality Modeling System (CMAQ) simulations were analyzed. CMAQ predictions showed that HCHO often extends higher into the atmosphere than NO_2, resulting in higher column FNRs than surface FNRs. Additionally, as seen in both CMAQ output and in situ aircraft vertical profiles, lofted NO_2 plumes from elevated point sources (such as coal-fired power plants) can lead to differences between surface and column FNR values. Surface measurements of HCHO and NO_2 made by the U.S. EPA at the Spaceport Sheboygan enhanced monitoring site during LMOS 2017 showed that the concentrations of both gases follow unique diurnal cycles. As a result, ozone production sensitivity and the associated FNR values also vary throughout the day. This reveals a limitation of using retrievals from current polar-orbiting satellite instruments to calculate FNRs because such datasets only capture HCHO and NO_2 concentrations at the satellite overpass time. Altogether, these findings suggest the need to apply different FNR ozone production regime thresholds when looking at satellite versus ground data. Additionally, this work highlights the need for higher precision HCHO and higher temporal resolution HCHO and NO_2 satellite retrievals to produce FNR datasets that capture the hourly fluctuations in ozone production sensitivity that should be considered when addressing ozone air pollution problems.

ACKNOWLEDGEMENTS

CONTENTS

LIST OF FIGURES

LIST OF TABLES

ACRONYMS, ABBREVIATIONS, & CHEMICAL FORMULAS

CAA	**C**lean **A**ir **A**ct
CDFs	**C**umulative **D**istribution **F**unction**s**
CH₄	*methane*
CMA	**C**hicago **M**etropolitan **A**rea
CMAQ	**C**ommunity **M**ultiscale **A**ir **Q**uality Modeling System
CO	*carbon monoxide*
CST	**C**entral **S**tandard **T**ime
D10	**D**uncan et al. 20**10**
DOAS	**D**ifferential **O**ptical **A**bsorption **S**pectroscopy
E_NOx	**E**missions of **NO**ₓ
ESA	**E**uropean **S**pace **A**gency
E_VOC	**E**missions of **VOC**s
FNR	**F**ormaldehyde to **N**itrogen Dioxide **R**atio (HCHO/NO₂)
GES DISC	**G**oddard **E**arth **S**ciences **D**ata & **I**nformation **S**ervices **C**enter
GLERL	**G**reat **L**akes **E**nvironmental **R**esearch **L**aboratory
H•	*hydrogen radical*
HCHO	*formaldehyde*
HNO₃	*nitric acid*
HOₓ	*hydrogen oxide radicals (HOₓ ≡ •OH + H• + ROO•)*
J20	**J**in et al. 20**20**

K-S Test	**K**olmogorov-**S**mirnov **Test**
km	**k**ilo**m**eter
L2	**L**evel **2**
LADCO	**L**ake Michigan **A**ir **D**irectors **C**onsortium
LMOS 2017	**L**ake **M**ichigan **O**zone **S**tudy **2017**
MCIP	**M**eteorology-**C**hemistry **I**nterface **P**rocessor
MDA8	**M**aximum **D**aily **8**-hour **A**verage
mol/cm^2	**mol**ecules per **c**enti**m**eter^2
N$_2$O$_5$	*dinitrogen pentoxide*
NAAQS	**N**ational **A**mbient **A**ir **Q**uality **S**tandards
NAAs	**N**on**A**ttainment **A**rea**s**
NASA	**N**ational **A**eronautics and **S**pace **A**dministration
nm	**n**ano**m**eter
NO	*nitrogen monoxide*
NO$_2$	*nitrogen dioxide*
NO$_x$	*nitrogen oxides ($NO_x \equiv NO + NO_2$)*
NO$_y$	*reactive nitrogen oxides ($NO_y \equiv NO_x$ + other reactive nitrogen species)*
NOAA	**N**ational **O**ceanic and **A**tmospheric **A**dministration
NYC	**N**ew **Y**ork **C**ity
O	*oxygen atom*
O$_2$	*oxygen molecule*
O$_3$	*ozone*

O$_x$	*odd oxygen species (O$_x$ ≡ O$_3$ + NO$_2$)*
•OH	*hydroxyl radical*
OMI	**O**zone **M**onitoring **I**nstrument
PAMS	**P**hotochemical **A**ssessment **M**onitoring **S**tations
ppb(v)	**p**arts **p**er **b**illion (by **v**olume)
RMSE	**R**oot **M**ean **S**quare **E**rror
ROO•	*peroxy radical*
S5P	**S**entinel-**5** **P**recursor
SD	**S**tandard **D**eviation
SIP	**S**tate **I**mplementation **P**lan
SNRs	**S**ignal-to-**N**oise **R**atio**s**
TEMPO	**T**ropospheric **E**missions**:** **M**onitoring of **PO**llution
TROPOMI	**TROPO**spheric **M**onitoring **I**nstrument
U.S. EPA	**U**nited **S**tates **E**nvironmental **P**rotection **A**gency
UTC	**U**niversal **T**ime **C**oordinated
VIIRS	**V**isible **I**nfrared **I**maging **R**adiometer **S**uite
VOCs	**V**olatile **O**rganic **C**ompound**s**
WRF	**W**eather **R**esearch and **F**orecasting Model

CHAPTER 1: INTRODUCTION & BACKGROUND

1.1 Ozone Pollution & Regulation in the United States

Ozone (O_3) is a naturally occurring gas in Earth's atmosphere comprised of three oxygen atoms. Despite existing in relatively small concentrations, ozone is an important trace gas that affects life on Earth. Approximately 90% of the ozone can be found in the stratosphere between about 10 and 50 kilometers (km) above Earth's surface in a region known as 'the ozone layer' (Gleason, 2008; **Figure 1.1**). Stratospheric ozone protects life on Earth by absorbing biologically harmful ultraviolet radiation from the sun, leaving only a small amount to reach the surface. The remaining 10% of atmospheric ozone is found in the troposphere below an altitude of 15 km (**Figure 1.1**).
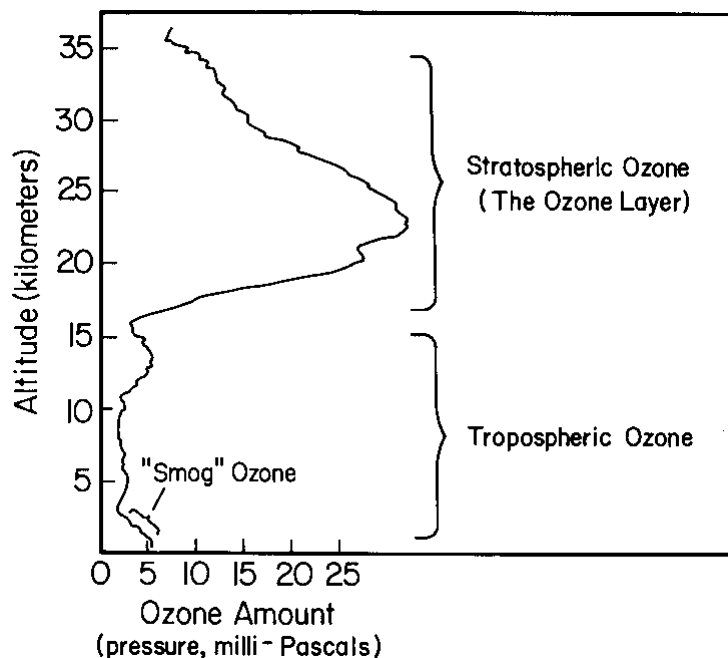
Figure 1.1 Typical vertical profile of ozone in the atmosphere (Gleason, 2008).

Unlike 'good' stratospheric ozone, tropospheric (or ground-level) ozone is 'bad' because of its toxicity to living systems (Gleason, 2008). Short-term exposure to elevated levels of ozone can cause various acute respiratory problems in humans, such as coughing, throat irritation, chest pain, and inflammation of airways (U.S. Environmental Protection Agency [EPA], 2021b). Long-term exposure can permanently damage lung tissue, decrease lung function, worsen chronic conditions like asthma (U.S. EPA, 2021b), and has been linked to increased mortality from respiratory and circulatory system illnesses (Jerrett et al., 2009; Turner et al., 2016). Ozone also damages plants and is estimated to cause global agricultural crop losses worth billions of U.S. dollars annually (Avnery et al., 2011).

To prevent these adverse effects, the U.S. EPA regulates tropospheric ozone levels through the enforcement of the Clean Air Act (CAA) and its subsequent amendments. In particular, the agency sets National Ambient Air Quality Standards (NAAQS) for ozone and other pollutants, which are atmospheric abundance levels above which concentrations of these pollutants are known to negatively impact human health and the environment (U.S. EPA, 2020a). Ground-level ozone NAAQS are currently set at an MDA8 value (the fourth-highest daily maximum 8-hour concentration, averaged across three consecutive years) of 70 parts per billion by volume (ppbv) (U.S. EPA, 2021a). Counties in the U.S. where ozone levels are observed to exceed this MDA8 value are deemed ozone nonattainment areas (NAAs) and are required by the CAA to develop state implementation plans (SIPs) to address the problem (U.S. EPA, 2020a). Ozone NAAs are found throughout the country, including the Lake Michigan region, which is the primary study area of this research (**Figure 1.2**).
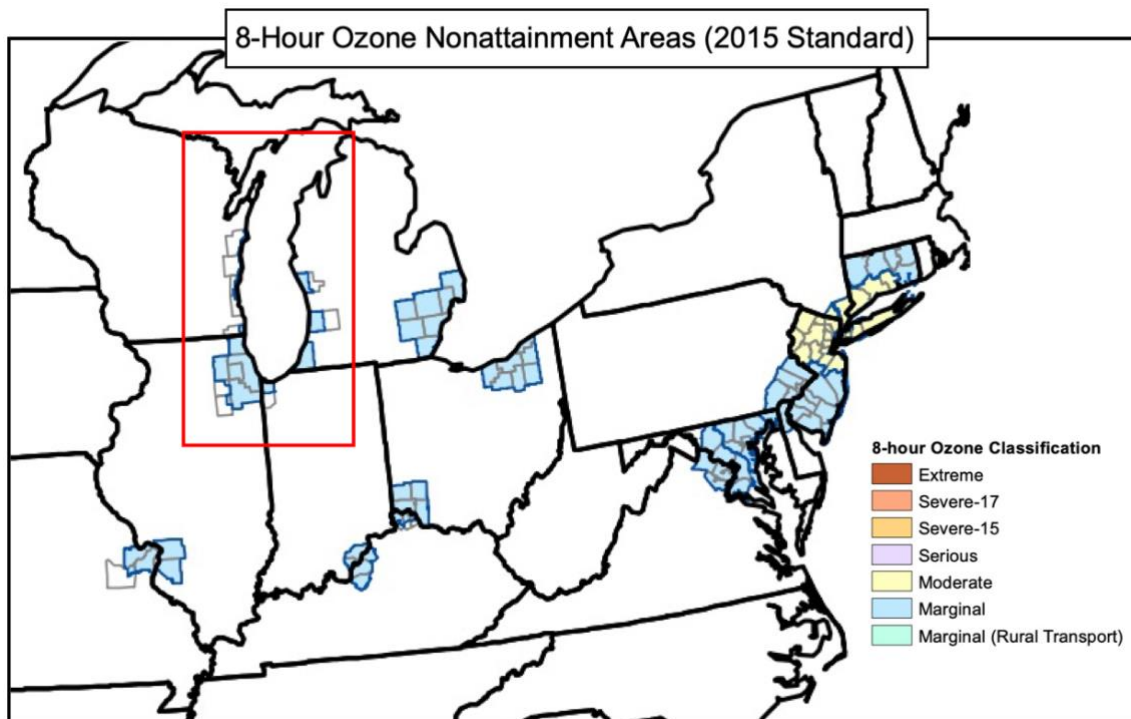
Figure 1.2 Map of ozone NAAs in the northeast quadrant of the United States; the domain within the red rectangle is the primary study area of this research (Adapted from U.S. EPA, 2021c).

1.2   Tropospheric Ozone Production Regimes

To address tropospheric ozone exceedance problems, it is important to know where ozone comes from. In polluted urban environments, ozone is a secondary pollutant formed in a series of hydrogen oxide radical (HO_x)-catalyzed ($HO_x \equiv$ hydroxyl radical [$\cdot OH$] + hydrogen radical [$H \cdot$] + peroxy radicals [$ROO \cdot$]) chain reactions involving the oxidation of methane (CH_4), nonmethane volatile organic compounds (VOCs), and carbon monoxide (CO) in the presence of nitrogen oxides ($NO_x \equiv$ nitrogen monoxide [NO] + nitrogen dioxide [NO_2]) and sunlight (Haagen-Smit, 1952; Jacob, 2000; Anenberg et al., 2009). The chain is initiated with the production of HO_x and propagated by the cycling of HO_x between its hydroxyl and peroxy radical forms (Jacob, 2000). The cycling of HO_x occurs through the oxidation of CO or hydrocarbons/volatile organic compounds; this cycle itself is catalyzed by the cycling of NO_x between its NO and NO_2 forms (Jacob, 2000). NO_2 can then be photolyzed to produce an oxygen atom (O), which goes on to react with an oxygen molecule (O_2) to form ozone (O_3) (Jacob, 2000). In densely populated areas, high NO_x and VOC emissions control the rate at which the catalytic cycles occur and thus ultimately affect the production rate of O_3 (Jacob, 1999). This complex series of ozone-producing reactions is illustrated in simplified form in **Figure 1.3**. Note that within the figure, the 'R' (such as in RH or RO_2) denotes either a radical or any group in which a carbon or hydrogen atom is attached to the rest of the molecule.
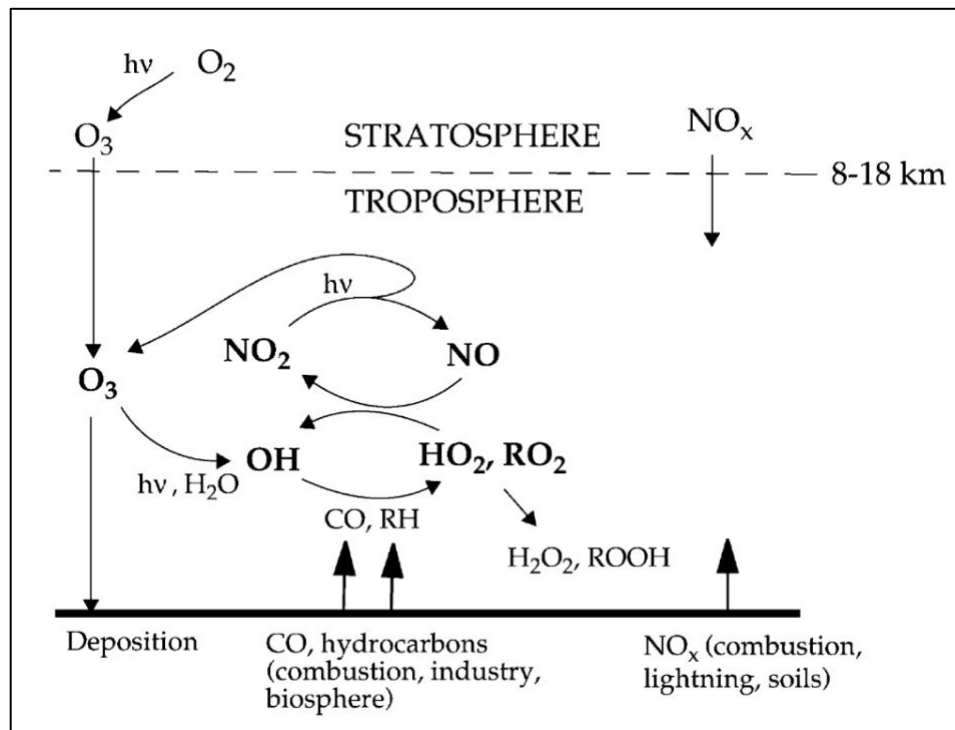
Figure 1.3 Schematic of tropospheric O_3 production (Jacob, 2000).

Many research studies have shown that the production rate of tropospheric ozone is a nonlinear function of the emissions/concentrations of NO_x and VOCs (Sillman, 1995; Kleinman et al., 2000; Goldberg et al., 2016; Mazzuca et al., 2016; Vermeuel et al., 2019). The nonlinear nature of ozone production is often demonstrated in a plot known as an ozone production isopleth, such as the one shown in **Figure 1.4**. This figure was adapted from one created by Vermeuel et al. (2019) and quantifies the response of odd oxygen ($O_x \equiv O_3 + NO_2$; colored shading) to changes in NO_x concentrations (y-axis) and VOC concentrations (x-axis). Ozone production isopleths reveal that O_3 production can be thought of as occurring in two regimes. In the NO_x-sensitive regime, reductions in NO_x emissions (E_{NOx}) lead to decreases in ozone production, while increases in E_{NOx} increase ozone production (lower right of **Figure**

1.4, green and red arrows, respectively). In the VOC-sensitive regime, reductions in VOC emissions (E_{VOC}) lead to decreases in ozone production, while increases in E_{VOC} increase ozone production (upper right of **Figure 1.4**, green and red arrows, respectively). Nonlinearity is seen in **Figure 1.4** as it demonstrates that a reduction in E_{NOx} in a NO_x-sensitive regime decreases ozone production (lower right green arrow), but a corresponding reduction in E_{NOx} within a VOC-sensitive regime increases the production of ozone (upper left purple arrow). Therefore, knowing which ozone production regime an ozone NAA falls into can be very informative for regulatory agencies that develop and enact O_3 control strategies based on the emissions of NO_x and VOCs within their regional airsheds.
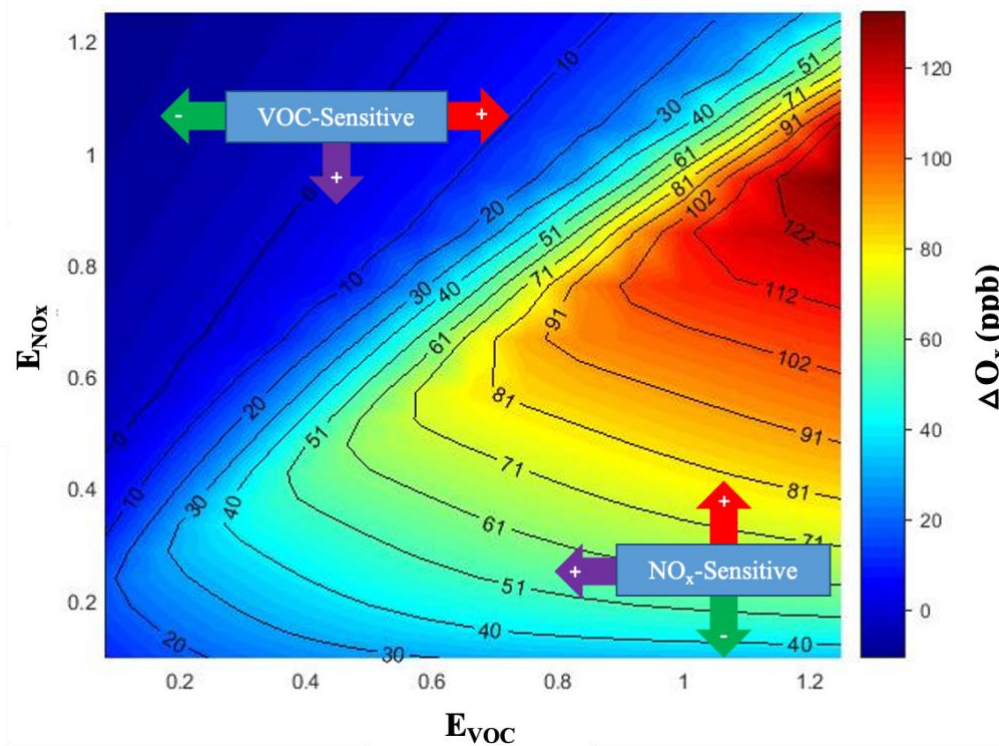
Figure 1.4 Example of an ozone production isopleth showing modeled O_x production over 5 hours as a function of NO_x and VOC emissions; NO_x and VOC emissions are shown relative to 1990 estimates for the Lake Michigan-Chicago region (Adapted from Vermeuel et al., 2019). The colored arrows are discussed in detail in the main text.

1.3   Research Motivation: The Formaldehyde to Nitrogen Dioxide Ratio

One of the ways that ozone production regimes can be identified is through indicator ratios that are calculated by dividing the concentrations of species involved in the chemical cycles that create ozone. Sillman (1995) found that the formaldehyde (HCHO; a VOC) to NO_y ratio is a viable indicator for ozone-NO_x-VOC sensitivity, where $NO_y \equiv NO_x$ + other reactive nitrogen species (e.g., nitric acid [HNO_3] and dinitrogen pentoxide [N_2O_5]). Note that the concentration of HCHO is often used as an indicator of VOC emissions since a sizable fraction of the oxidation reactions between •OH and VOCs produces HCHO within the HO_x catalytic cycle that is discussed in **Section 1.2** (Valin et al., 2016). Sillman's chemical modeling work (1995) showed that higher HCHO/NO_y values are correlated to NO_x-sensitive ozone production while lower HCHO/NO_y values are correlated to VOC-sensitive ozone production. Tonnesen & Dennis (2000) extended Sillman's work and found that the formaldehyde to nitrogen dioxide ratio (HCHO/NO_2; referred to as 'FNR' for the rest of this paper) is a more useful indicator of ozone-NO_x-VOC sensitivity since HCHO and NO_2 have similar lifetimes on the order of hours, while NO_y has a lifetime on the order of days. Using species with similar lifetimes in the indicator ratio better represents the interactions between the HO_x and NO_x catalytic cycles that result in ozone production (Tonnesen & Dennis, 2000).

The satellite remote sensing research community has adapted this concept and used FNRs to assess ozone production regimes for various regions across the globe (Martin et al., 2004; Duncan et al., 2010; Jin & Holloway, 2015; Chang et al., 2016; Jin et al., 2017; Jin et al., 2020). Many of these studies used satellite-based retrievals of HCHO and NO_2 from the Ozone Monitoring Instrument (OMI) onboard the National Aeronautics and Space

Administration (NASA) Aura satellite to calculate satellite-based FNRs. Using a combination of chemical modeling and satellite data analyses, these studies reported similar correlations to those that previous studies found between ozone production sensitivity and the HCHO to NO_y ratio (Sillman, 1995) or HCHO to NO_2 ratio (Tonnesen & Dennis, 2000). Specifically, higher FNR values are correlated to NO_x-sensitive ozone production while lower FNR values are correlated to VOC-sensitive ozone production.

Despite this general agreement, there are differences among studies in what FNR values correspond to the two ozone production regimes. For example, Duncan et al. (2010) [referred to as 'D10' for the rest of this work] found that OMI FNRs less than 1 indicate VOC sensitivity, FNRs between 1 and 2 indicate a transition between VOC and NO_x sensitivities ('the transition zone'), and FNRs greater than 2 indicate NO_x-sensitive ozone production (**Table 1.1**). A more recent study by Jin et al. (2020) [referred to as 'J20' for the rest of this work], suggests that OMI FNRs less than 3.2 indicate VOC-sensitive ozone production, FNRs between 3.2 and 4.1 indicate the transition zone, and FNRs greater than 4.1 indicate NO_x-sensitive ozone production (**Table 1.1**). Although both studies utilize satellite retrievals from Aura OMI, the J20 threshold for VOC sensitivity is greater by a factor of ~3 than the D10 threshold while the J20 threshold for NO_x sensitivity is greater by a factor of ~2 than the D10 threshold.

Table 1.1 Comparison of D10 & J20 FNR thresholds for different O_3 production regimes

O_3 Production Regime	D10 Thresholds	J20 Thresholds
VOC-sensitive	FNR < 1	FNR < 3.2
Transition zone	1 < FNR < 2	3.2 < FNR < 4.1
NO_x-sensitive	FNR > 2	FNR > 4.1

These highlighted studies have different threshold values because of the way the FNR threshold values were determined. D10 utilized Community Multiscale Air Quality Modeling System (CMAQ) simulations and the NASA Langley Research Center time-dependent photochemical box model and applied radical versus NO_x sinks as an indicator of ozone-NO_x-VOC sensitivity to determine FNR thresholds based on surface and boundary layer (up to altitudes of 0.2-2 km) concentrations. However, the use of chemical modeling to determine FNR threshold values has potential drawbacks because of uncertainties in the model predictions. Satellite data, on the other hand, retrieves full tropospheric column concentrations (up to altitudes of 9-17 km). In other words, surface and boundary layer FNR values may be different than those of the full tropospheric column. The potential differences between column FNRs calculated from satellite data and surface FNRs calculated from in situ data provides a source of motivation for this research.

In contrast to D10, J20 connected OMI-derived FNRs to high ozone event probabilities calculated from in situ ground monitor data to determine FNR threshold values for different ozone production regimes. Differences between the D10 and J20 threshold values (derived from the distinctive ways that they were determined) can result in different interpretations of ozone production sensitivity for the same ozone nonattainment area depending on which thresholds are used to analyze satellite FNRs. The primary motivation of this research study is to examine how J20 advances the work of D10 by analyzing the differences in ozone-NO_x-VOC sensitivity indicated by each study's FNR threshold values when applied to the Lake Michigan region.

1.4   Research Objectives

To build upon the work of D10 and J20 as well as provide further insight on the differences between surface and column FNRs, this study investigates three major research questions:

(1) What do FNRs calculated from satellite retrievals indicate about ozone-NO_x-VOC sensitivity in the Lake Michigan region, and how do these interpretations of ozone production sensitivity differ depending on which FNR threshold values (D10 or J20) are used?

(2) How do satellite-based FNRs compare to ground-based FNRs?

(3) What accounts for the differences between satellite-based and ground-based FNRs?

To answer these questions, monthly composited FNRs for the 2018 and 2019 ozone seasons calculated using satellite-based retrievals of HCHO and NO_2 were compared to FNRs calculated using ground-based observations of HCHO and NO_2. Additionally, field data from the Lake Michigan Ozone Study (LMOS) 2017 field campaign (Abdioskouei et al., 2019) and high-resolution LMOS 2017 air quality simulations were analyzed to investigate possible causes for the numerical differences between satellite and ground FNRs.

The remainder of this thesis is organized as follows. Chapter 2 provides a description of the satellite, in situ, and air quality modeling datasets used in this research as well as the methodology for processing the data. Discussion and analysis of the results and limitations of this work are presented in Chapter 3. Finally, a summary of the study's findings and broader implications are discussed in Chapter 4.

CHAPTER 2: DATASETS & METHODS

2.1   Dataset Summary

This study uses a variety of datasets, including: (1) satellite retrievals of HCHO and NO$_2$ from the Sentinel-5 Precursor (S5P) satellite's TROPOspheric Monitoring Instrument (TROPOMI); (2) in situ ground measurements of HCHO and NO$_2$ from U.S. EPA Photochemical Assessment Monitoring Stations (PAMS); (3) in situ surface measurements of HCHO and NO$_2$ from the LMOS 2017 field campaign Spaceport Sheboygan EPA ground site; (4) LMOS 2017 CMAQ air quality simulations; and (5) in situ vertical profiles of NO$_2$ measured from Scientific Aviation aircraft.

2.2   Satellite Data: S5P TROPOMI

To calculate satellite FNRs, S5P TROPOMI Version 1 tropospheric NO_2 (Koninklijk Nederlands Meteorologisch Instituut [KNMI], 2018, 2019) and HCHO (German Aerospace Center [DLR], 2019a, 2019b) orbital level 2 (L2) data for the ozone seasons of 2018 and 2019 were downloaded from the NASA Goddard Earth Sciences Data and Information Services Center (GES DISC). The S5P satellite has a polar, sun-synchronous orbit and provides global daily data approximately at 13:30 local solar time (Zehner, n.d.). TROPOMI is an ultraviolet-visible-near infrared-shortwave infrared nadir-viewing grating spectrometer with the following specifications: a spectral range of 270-500, 675-775, and 2305-2385 nanometers (nm); a spectral resolution of 0.25-1.1 nm; and an original spatial resolution of 3.5 x 7 km^2 (Zehner, n.d.), which was increased to 3.5 x 5.5 km^2 on August 6, 2019 (Geffen et al., 2020). TROPOMI retrievals have signal-to-noise ratios (SNRs) that are similar to OMI but with much higher spatial resolution (Veefkind et al., 2012; De Smedt et al., 2018). These TROPOMI datasets were used to create FNR composites, which were evaluated using the D10 and J20 OMI-based thresholds.

2.2.1   Satellite FNRs: TROPOMI Ozone Season Monthly Composites

TROPOMI retrievals of HCHO are primarily derived from the instrument's spectral Band 3 (range: 310-405 nm), while NO_2 retrievals are derived from spectral Band 4 (range: 405-500 nm) (Veefkind et al., 2012; De Smedt et al., 2018; Geffen et al., 2019). Both bands have a minimum signal-to-noise ratio (SNR) of 800-1000 (Veefkind et al., 2012). However, HCHO has an optical density that is an order of magnitude smaller than that of NO_2, resulting in HCHO retrievals with lower SNRs than NO_2 retrievals (De Smedt et al., 2018). To reduce the impacts of the lower SNRs of TROPOMI HCHO retrievals and to allow for the analysis of general spatial patterns in FNR values, gridded monthly TROPOMI NO_2 and HCHO 'clear sky' (cloudy radiance fraction < 30%) composites were constructed using quality controlled L2 retrievals based on the recommended qa_value > 0.75 from the TROPOMI README files for NO_2 (Eskes et al., 2020) and HCHO (De Smedt et al., 2020). Additional 'detection limit' filters of 1.5 x 10^{15} molecules/cm^2 (mol/cm^2) for NO_2 (Duncan et al., 2010) and 1.8 x 10^{15} mol/cm^2 for HCHO (Chance [Ed.], 2002) were applied to the L2 orbital retrievals used in the monthly composites. It is important to note that these detection limit values are for OMI data, but it is assumed that the same filter values can be applied to TROPOMI data because of the similarities in the SNRs of both instruments.

Since part of this research was conducted in collaboration with the Lake Michigan Air Directors Consortium (LADCO), the gridded monthly composites of HCHO and NO_2 were constructed using Meteorology-Chemistry Interface Processor (MCIP) files from the LADCO modeling platform 12 x 12 km^2 grid with a Lambert Conformal Conic projection. The LADCO modeling platform also has a 4 x 4 km^2 grid, but it was not utilized because the 'test'

composites created using this grid were still 'noisy' despite using a month of data for each composite. This is due to the quality control and detection limit filtering that resulted in not enough TROPOMI retrievals being averaged into the 4 x 4 km^2 grid cells. The 12 x 12 km^2 grid allowed for more satellite data to be averaged into the larger grid cells, which helped to reduce noise in the monthly composites of HCHO.

The TROPOMI composites cover an area that extends north into southern Canada, east to the East Coast, south to the northern portions of the Gulf states, and west covering portions of central states such as Nebraska (**Figure 2.1**). The gridded monthly HCHO and NO$_2$ composites were produced for the ozone seasons of 2018 and 2019, covering the periods of June to October 2018 and May to October 2019. A May 2018 composite was not created because TROPOMI HCHO data were not available for the entire month. Finally, monthly satellite FNR composites were constructed by dividing the monthly composite values of HCHO and NO$_2$ for each grid cell.
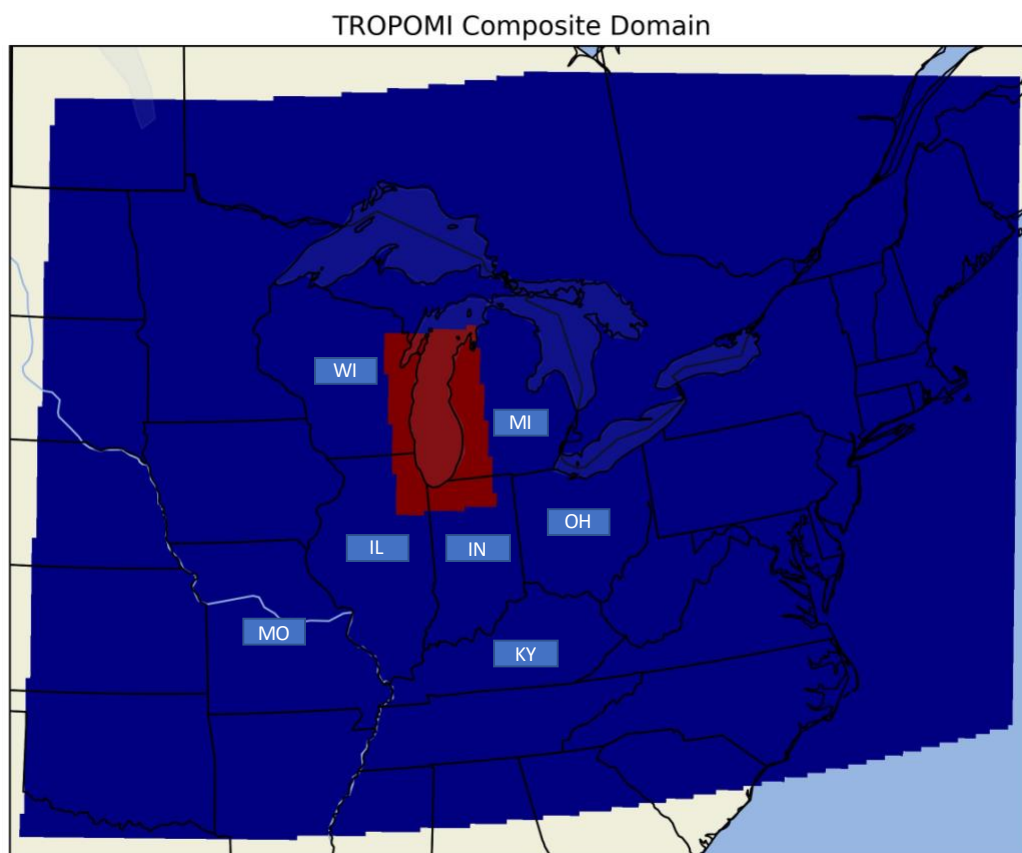
Figure 2.1 This map shows the full spatial domain of the TROPOMI composites in dark blue. The inner red domain highlights the Lake Michigan region, which is the primary study area of analysis for much of this work. The labeled states are ones for which ozone exceedance day composites were created or ground FNRs were calculated.

2.2.2   Satellite FNRs: TROPOMI Ozone Exceedance Day Composites

In addition to creating monthly composites of TROPOMI data for the ozone seasons of 2018 and 2019, ozone exceedance day composites for individual nonattainment areas were also constructed. This work defines an 'ozone exceedance day' as having at least one ground monitor within an NAA measuring an MDA8 value greater than the ozone NAAQS of 70 ppbv. Collaborators at LADCO provided ozone exceedance data (Donna Kenski, personal communication, April 1, 2020) for several NAAs, including Chicago, Illinois; Louisville, Kentucky; Detroit, Michigan; Western Michigan, Michigan; St. Louis, Missouri; Cincinnati, Ohio; Cleveland, Ohio; Columbus, Ohio; and Sheboygan, Wisconsin (**Figure 2.1**). Most of the ozone exceedance days for the NAAs occurred in 2018. The composites were created following the same methodology explained in **Section 2.2.1** but only using TROPOMI data for the identified ozone exceedance days for each individual NAA. Although ozone exceedance day composites were created for all the NAAs listed above, subsequent analyses focus on Chicago, Illinois, as it falls within the primary study area of this work and had the largest number of ozone exceedance days (33) within the study period, resulting in the most statistically robust composite created.

2.3   Ground FNRs: EPA PAMS

Collaborators at LADCO also provided EPA PAMS data (Donna Kenski, personal communication, April 15, 2020; U.S. EPA, 2020b, 2020c) for use in the calculation of ground FNRs. This dataset contains NO_2 concentrations measured in 1-hour sampling intervals and HCHO concentrations measured in 8-hour or 24-hour sampling intervals for various EPA PAMS sites across the United States. To compare the ground-based ratios to the satellite-based data, the EPA PAMS data were filtered to sites within the TROPOMI composite domain (**Figure 2.1**) with concurrent HCHO and NO_2 measurements. This filtering process resulted in the selection of four sites for analysis: Site 3103 in Cook County, Illinois; Site 78 in Marion County, Indiana; Site 15 in Wayne County, Michigan; and Site 85 in St. Louis City County, Missouri. After identifying the analysis sites, the EPA PAMS HCHO data were converted (assuming standard pressure and temperature) from their original units of $\mu g/m^3$ to the same units as the NO_2 data (ppb), and the 1-hour NO_2 and 8-hour/24-hour HCHO measurements were averaged to get monthly values. These monthly values were then divided to get monthly FNR values in order to compare them to the previously generated monthly composites of TROPOMI data. The nearest TROPOMI monthly composite grid boxes for each EPA PAMS site were identified and used to extract the satellite-based ratios for comparison.

2.4   LMOS 2017 Field Campaign Data

LMOS 2017 was a collaborative field campaign coordinated by LADCO dedicated to studying the production of ozone along the western shore of Lake Michigan from May to June 2017 (Abdioskouei et al., 2019). Participants included individuals and groups from academic institutions, state and federal agencies, non-profit organizations, and private companies (e.g., University of Wisconsin-Madison, University of Iowa, University of Minnesota, Wisconsin Department of Natural Resources, Lake Michigan Air Directors Consortium, U.S. EPA, NASA, Electric Power Research Institute, Scientific Aviation, etc.). LMOS 2017 field campaign data were downloaded from the LMOS 2017 data archive on the NASA Airborne Science Data for Atmospheric Composition website, and the data were utilized to investigate possible causes for the differences between satellite and ground FNRs. Specifically, in situ measurements taken from airborne and fixed ground-based observational platforms as well as air quality modeling work were used. More details about these datasets are provided in the following subsections.

2.4.1 LMOS 2017 Spaceport Sheboygan EPA Ground Site FNRs

To explore the impact of 24-hour HCHO sampling on the ground-based EPA PAMS FNRs, in situ HCHO and NO_2 measurements from the LMOS 2017 Spaceport Sheboygan EPA enhanced monitoring site (U.S. EPA Office of Research and Development, National Exposure Research Laboratory, 2017, 2018) were analyzed. The measurements at the Spaceport Sheboygan ground site were collected at a high temporal resolution of one minute, which allowed for the averaging of in situ HCHO and NO_2 data into block intervals representing different sampling intervals of 5 minutes, 1 hour, and 24 hours. Additionally, because the data were collected for 27 days between May 26 and June 21, 2017, the different block intervals were then composited to get 'monthly' average ground concentrations of HCHO and NO_2. Finally, these 'monthly' average ground concentrations were divided to get 'monthly' average FNR values. This analysis provided additional context to comparisons between the EPA PAMS and TROPOMI FNR data.

2.4.2   LMOS 2017 CMAQ Simulations & Scientific Aviation NO$_2$ Data

Output data from LMOS 2017 CMAQ simulations were analyzed to examine the differences in the vertical profiles of HCHO and NO$_2$, which can lead to discrepancies between column and ground FNRs. These simulations were conducted during a project that has been funded by the NASA Applied Sciences Health and Air Quality Program to perform air quality modeling assessments utilizing observations from LMOS 2017 (project title: *A satellite constrained meteorological modeling platform for LADCO States SIP development*; PI: Jason Otkin). The LMOS 2017 field campaign meteorological modeling platform was developed using a series of sensitivity experiments utilizing the Weather Research and Forecasting (WRF) model. The most optimized framework incorporated the following: (1) Thompson et al. microphysics (2008), (2) the Yonsei University Planetary Boundary Layer scheme (Hu et al., 2013), (3) the Noah Land Surface Model (Ek et al., 2003), (4) lake surface temperature retrievals from the National Oceanic and Atmospheric Administration (NOAA) Great Lakes Environmental Research Laboratory (GLERL), (5) soil moisture and temperature analyses provided by the NASA Short-term Prediction Research and Transition Center, (6) Visible Infrared Imaging Radiometer Suite (VIIRS) green vegetation fraction dataset (Myneni, 2018), and (7) the nudging of temperature, moisture, and horizontal winds only above 2 km. The latest simulations from this project have output with a high spatial resolution of 1.3 km^2, and the interactions between air pollution emissions and atmospheric dynamics (e.g., lake breeze) seen in the modeling results are comparable to field measurements taken during LMOS 2017 (Otkin et al., 2021). Vertical profiles of HCHO and NO$_2$ from these CMAQ simulations were analyzed as curtain plots over the grid box containing Spaceport Sheboygan. Model NO$_2$ data were also

compared to in situ Scientific Aviation flight observations of NO_2 (Conley, 2019) in order to evaluate model accuracy regarding lofted features seen in the NO_2 curtain plots. To do this, the gridded CMAQ model NO_2 values were interpolated via a nearest neighbor technique to the latitude, longitude, altitude, and time of the in situ flight observations.

CHAPTER 3: RESULTS & DISCUSSION

3.1   TROPOMI Ozone Season Monthly Composites: Full Domain

Gridded monthly clear sky HCHO, NO$_2$, and FNR composites were produced for the periods June to October 2018 and May to October 2019. **Figures 3.1 and 3.2** show the results of the monthly NO$_2$ and HCHO composites for July 2018 and July 2019, respectively. Peak July clear sky tropospheric NO$_2$ columns occur over New York City (NYC) and reach 12 x 10^{15} mol/cm^2 in 2018 and 7.1 x 10^{15} mol/cm^2 in 2019. Peak July clear sky tropospheric HCHO columns (approximately 20 x 10^{15} mol/cm^2) occur over Oklahoma, Arkansas, and Missouri in 2018 and along the eastern seaboard during 2019. The number of NO$_2$ and HCHO observations per grid box varies considerably across the analysis domain. This is due to a combination of the distribution of cloudiness as well as the detection limit threshold that was applied in the filtering of the L2 retrievals. The highest density of NO$_2$ observations per grid box occurs in urban areas, and there are a fairly low number of NO$_2$ retrievals above the detection limit over rural areas. Grid boxes with a low number of binned NO$_2$ retrievals have 'noisy' composite values and thus questionable FNR values (e.g., in Ontario, Canada, north of the Minnesota border). However, this is not a major issue for this study because the subsequent analyses focus on regions with relatively high numbers of binned NO$_2$ retrievals. The density of HCHO observations is generally higher than that of NO$_2$ in both rural and urban areas. This is reasonable since HCHO is a secondary product of both biogenic and anthropogenic VOCs and also has primary anthropogenic emissions sources.

July 2018
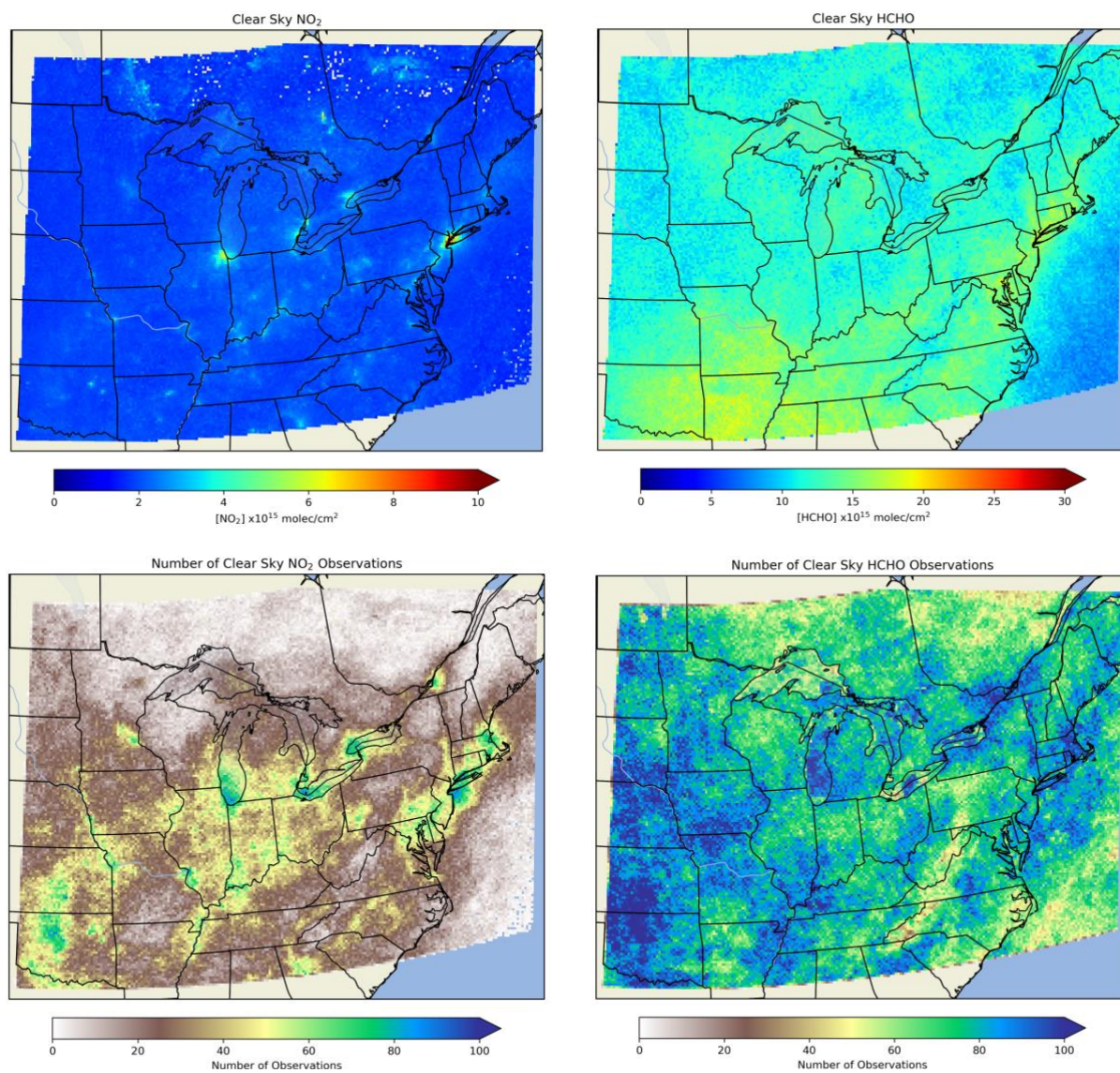
Figure 3.1 July 2018 composites of TROPOMI data for NO_2 (x 10^{15} mol/cm^2, upper left),

HCHO (x 10^{15} mol/cm^2, upper right), the number of composited NO_2 retrievals per grid box

(lower left), and the number of composited HCHO retrievals per grid box (lower right).

July 2019
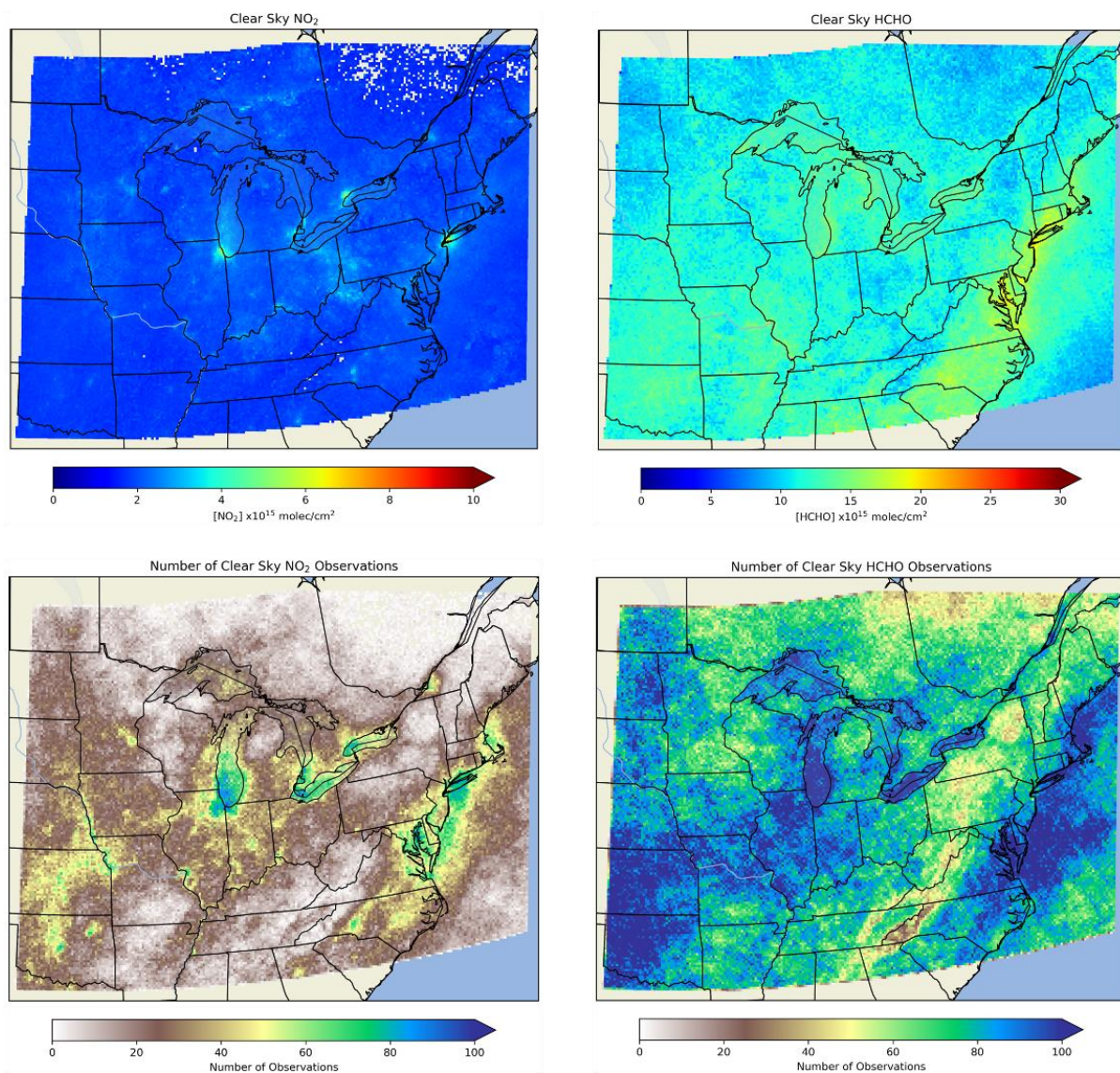
Figure 3.2 July 2019 composites of TROPOMI data for NO_2 (x 10^{15} mol/cm^2, upper left), HCHO (x 10^{15} mol/cm^2, upper right), the number of composited NO_2 retrievals per grid box (lower left), and the number of composited HCHO retrievals per grid box (lower right).

Figure 3.3 shows the composite TROPOMI FNRs for July 2018 and 2019. The minimum value of 1.5 occurs over NYC in 2018 while the minimum value of 2.2 occurs over Chicago in 2019. According to the D10 thresholds, this TROPOMI-based FNR analysis suggests that no urban centers within the domain are VOC-sensitive (FNR < 1) and that major urban centers (Chicago and NYC) fall into the transition between NO_x and VOC sensitivities during July 2018 and 2019. However, the J20 thresholds suggest that Chicago and NYC fall in the VOC-sensitive ozone production regime (FNR < 3.2) during July 2018 and 2019. When using the J20 thresholds to interpret the composites, more of the domain is classified as VOC-sensitive or in the transition zone as compared to using the D10 thresholds, which classifies much of the domain as NO_x-sensitive. When looking at the results of all the monthly composites (not shown), the July 2019 minimum FNR value of 2.2 was the largest minimum during the analysis period. The lowest minimum ratios occur in NYC in October, reaching 0.7 and 0.9 in 2018 and 2019, respectively.
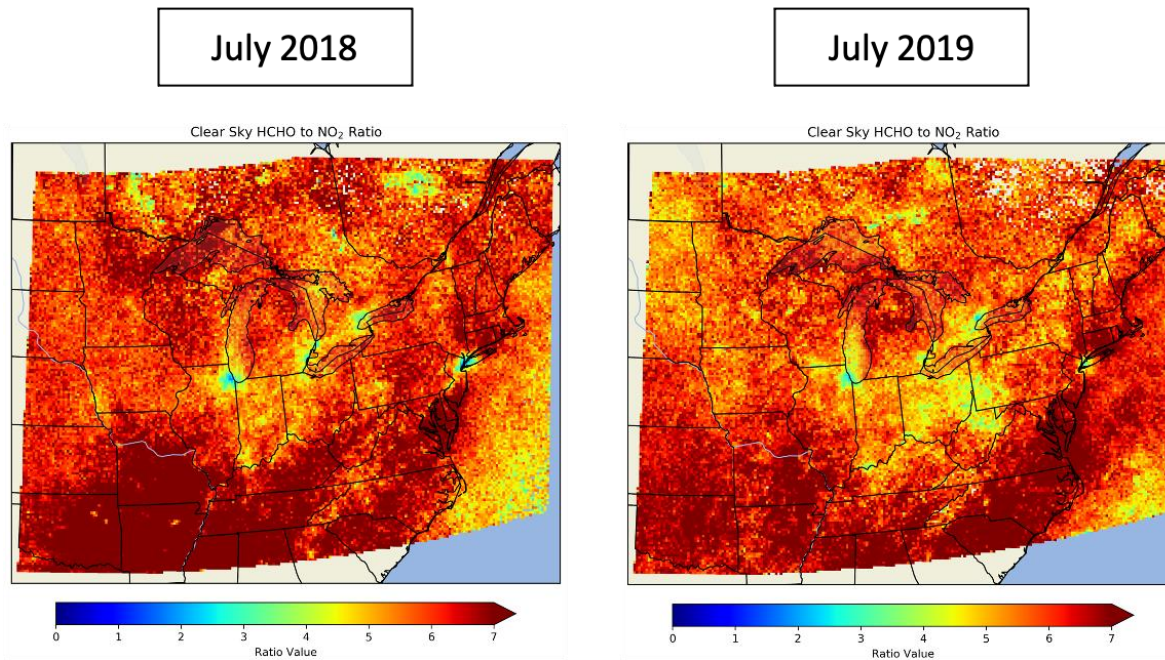
Figure 3.3 TROPOMI FNR composites for July 2018 (left) and July 2019 (right).

A combined 2018-2019 ozone season FNR composite (**Figure 3.4**) was created by computing the weighted mean (based on the number of observations per grid box per month) for HCHO and NO_2 during June-October 2018 and May-October 2019 and then computing the FNRs by dividing the weighted means. The minimum ratio occurs over NYC (1.64) with Chicago also slightly less than 2 (1.92), placing the urban centers in the transition zone according to D10 but in the VOC-sensitive regime according to J20. Detroit, Toronto, and Montreal show values between 2 and 3, making these urban centers in the D10 NO_x-sensitive regime and the J20 VOC-sensitive regime. Ozone season compositing shows a number of urban areas in the southeast US with lower ratios (~4.5) than the southeast rural areas but still within the NO_x-sensitive regime for both the D10 and J20 thresholds. As seen in the analysis

of both **Figures 3.3 and 3.4**, interpretations of ozone production sensitivity are vastly different

depending on which thresholds (D10 or J20) are used.
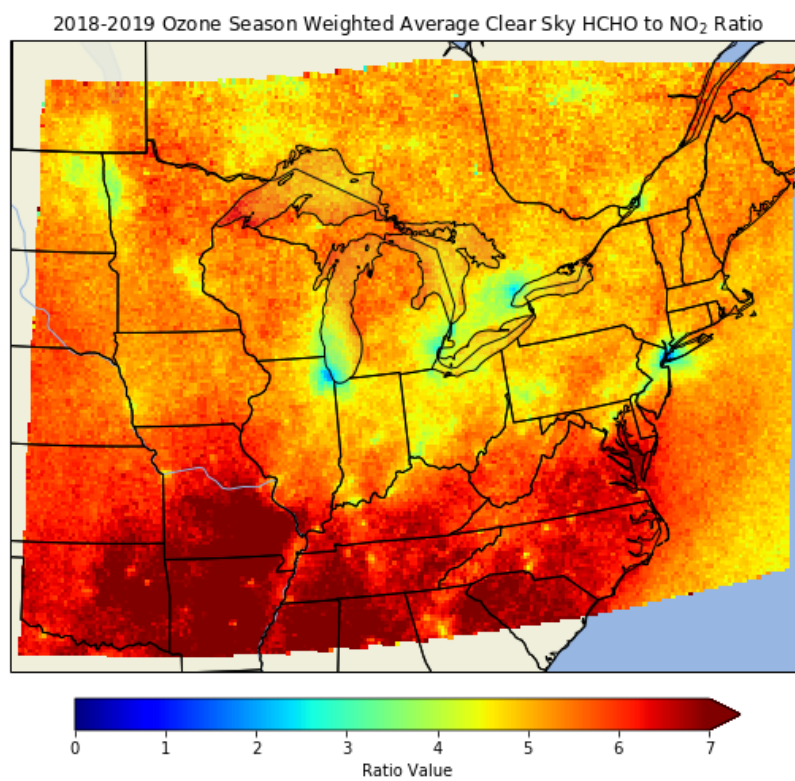
Figure 3.4 FNR composite for the 2018 and 2019 ozone seasons combined.

3.2   TROPOMI Ozone Season Monthly Composites: Lake Michigan Region

   Figure 3.5 displays the results from **Figures 3.1-3.3** when zoomed into the Lake Michigan region, which is defined as between latitudes 41^oN and 45.3^oN and longitudes 88.6^oW and 85.49^oW. **Table 3.1** lists the summary statistics of HCHO, NO_2, and FNR values for this domain. In general, HCHO is more uniformly distributed but noisier than NO_2. The highest values of HCHO can be seen along the eastern coast of Lake Michigan, resulting in the highest FNRs within the domain. The highest values of NO_2 are found in the Chicago Metropolitan Area (CMA), resulting in the lowest FNRs in the region. In July 2018, the CMA had a minimum ratio value of 1.79, placing it in the D10 transition zone but the J20 VOC-sensitive regime. In July 2019, the minimum ratio value within the CMA increased to 2.21 due to a decrease in NO_2, indicating NO_x-sensitive ozone production according to D10 but still within the J20 VOC-sensitive regime. Outside of the CMA, FNRs are greater than 2, making ozone production in the rest of the domain NO_x-sensitive for both July 2018 and 2019 according to D10. Using the J20 thresholds, a larger area is classified as being in the transition zone surrounding the CMA in July 2018 and 2019, but just as using the D10 thresholds, most of the Lake Michigan domain is classified as NO_x-sensitive. The differences seen between the TROPOMI composites of HCHO and NO_2 in July 2018 and 2019 (top and middle rows, right column of **Figure 3.5**) can be due to many reasons, such as differences in emissions (e.g., reductions in NO_2 emissions) and meteorological conditions (e.g., higher temperatures and varying transport patterns). Annual changes in NO_2 in Chicago and over Lake Michigan are evident and suggest transport differences between 2018 and 2019. The difference between the FNR composites (bottom row, right column of **Figure 3.5**) appears to look more like the

difference in HCHO rather than NO_2, suggesting that variation in HCHO is the primary driver of the variation in FNR values between July 2018 and 2019.

Table 3.1 Summary statistics of HCHO, NO_2, and FNR Composite Data in Figure 3.5

July 2018	Minimum	Mean	Maximum
HCHO (mol/cm²)	8.56×10^{15}	12.10×10^{15}	15.60×10^{15}
NO_2 (mol/cm²)	1.76×10^{15}	2.31×10^{15}	6.44×10^{15}
FNR	1.79	5.40	7.28
July 2019	Minimum	Mean	Maximum
HCHO (mol/cm²)	9.56×10^{15}	12.70×10^{15}	15.20×10^{15}
NO_2 (mol/cm²)	1.71×10^{15}	2.37×10^{15}	5.89×10^{15}
FNR	2.21	5.50	7.79
Difference (2019 - 2018)	Minimum	Mean	Maximum
HCHO (mol/cm²)	-4.28×10^{15}	0.57×10^{15}	4.32×10^{15}
NO_2 (mol/cm²)	-2.00×10^{15}	0.06×10^{15}	1.04×10^{15}
FNR	-1.80	0.10	2.05
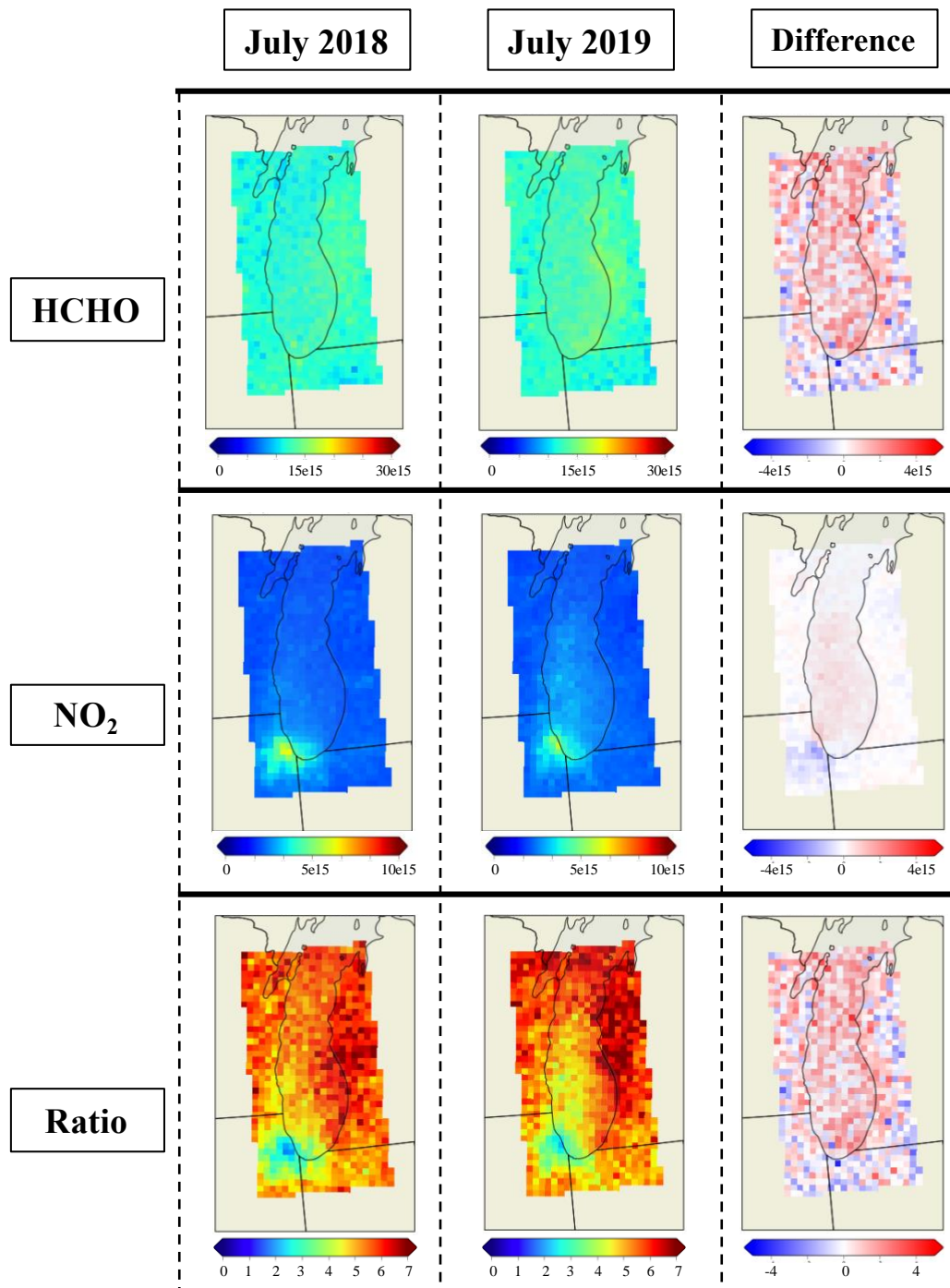
Figure 3.5 Lake Michigan region TROPOMI composites of HCHO (top row), NO₂ (middle row), and FNRs (bottom row) for July 2018 (left column), July 2019 (middle column), and the difference between the years (2019 – 2018, right column).

3.3 TROPOMI Ozone Exceedance Day Composites: Lake Michigan Region

Ozone exceedance composites were created by gridding TROPOMI HCHO and NO_2 data collected during ozone exceedance events that occurred in the ozone NAAs listed in **Section 2.2.2**. Although results were generated for all the NAAs, only the results for the Chicago NAA are discussed in the rest of this section. **Figure 3.6** focuses on the Lake Michigan region (as defined in the previous section) and shows a comparison between HCHO, NO_2, and FNRs for the combined 2018-2019 ozone season composite and for the Chicago NAA ozone exceedance day composite. The Chicago NAA had the largest number of ozone exceedance events (33) of all the NAAs during 2018 and 2019 and consequently has the most robust statistics.
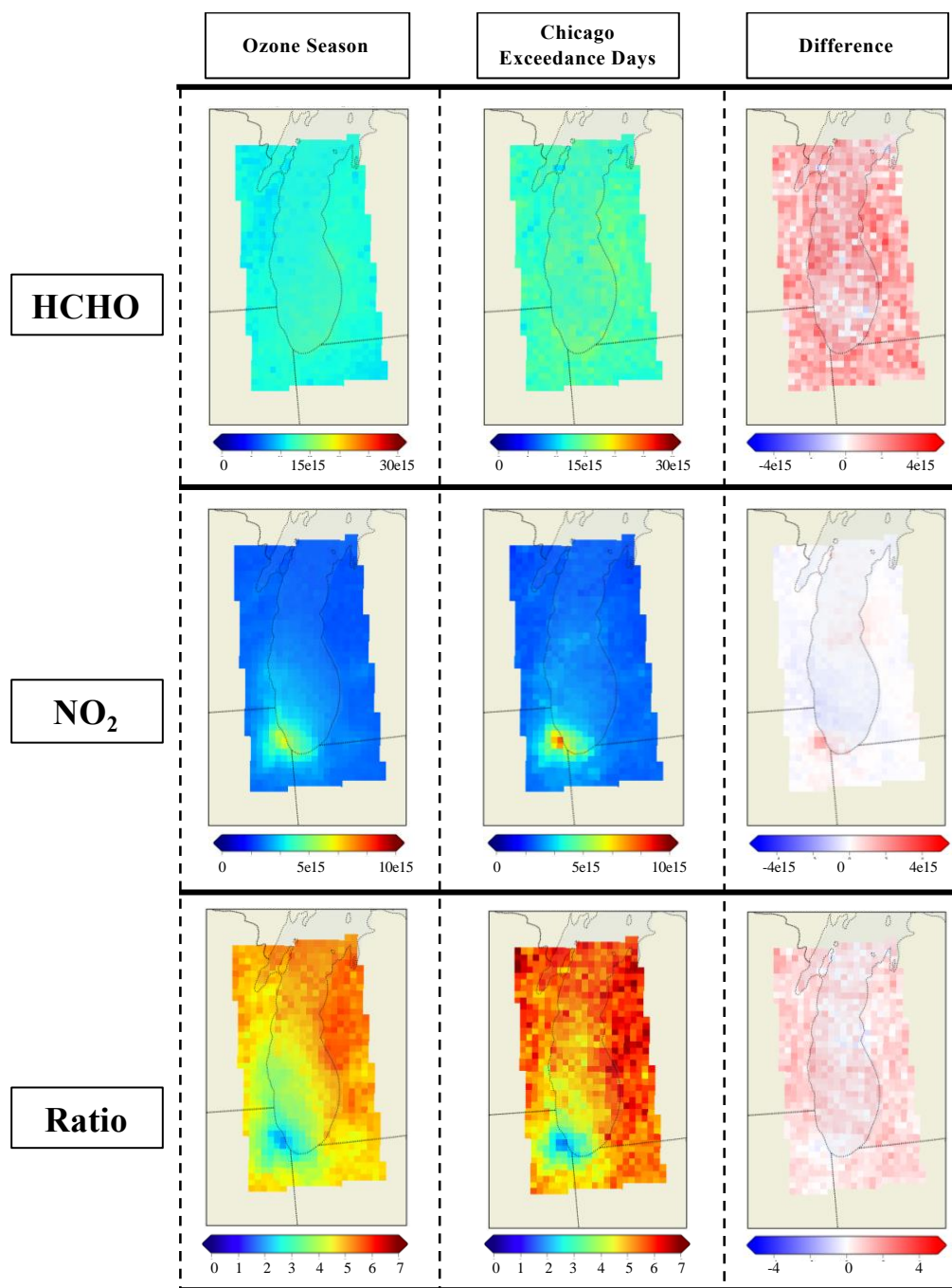
Figure 3.6 TROPOMI composites of HCHO (top row), NO₂ (middle row), and FNRs

(bottom row) for the combined 2018 and 2019 ozone seasons (left column), ozone

exceedance events in the Chicago NAA (middle column), and the difference (exceedance

composite – ozone season; right column).

The minimum FNR during 2018 and 2019 over Chicago is 12% lower (1.73) during ozone exceedance days than the minimum for the average ozone season (1.92). However, the largest differences are associated with larger FNR values in non-urban areas during ozone exceedance events. This is caused by larger background HCHO abundances (top row, right column of **Figure 3.6**) and is likely due to increased temperatures during ozone exceedance events, which lead to increased biogenic VOC emissions and thus increased ozone production (Sillman & Samson, 1995). To investigate this further, histograms and cumulative distribution functions (CDFs) (**Figure 3.7**) of HCHO, NO_2, and FNR values were plotted for the ozone season and during Chicago ozone exceedance events within the domain shown in **Figure 3.6**. To determine whether the differences between the ozone season and ozone exceedance distributions were statistically significant, two-sample Kolmogorov-Smirnov (K-S) tests were performed. The two-sample K-S test assesses whether the two sample distributions come from the same population distribution (Heckert, 2016). At a confidence level of 95%, the null hypothesis (that the sample distributions come from the same population distribution) is rejected when the p-value is less than 0.05. The results of the two-sample K-S tests are shown in **Table 3.2**.

Table 3.2 Summary of two-sample K-S test results performed on data in Figure 3.7

Variable	p-value	K-S statistic	Result
HCHO	8.0×10^{-184}	0.680	Significant
NO_2	0.196	0.053	Not Significant
Ratio	2.6×10^{-49}	0.363	Significant

Values during Ozone Season	Values during Chicago Ozone Exceedance Days	D10 --VOC-Sensitive-- FNR < 1	D10 --NOₓ-Sensitive-- FNR > 2	J20 --VOC-Sensitive-- FNR < 3.2	J20 --NOₓ-Sensitive-- FNR > 4.1
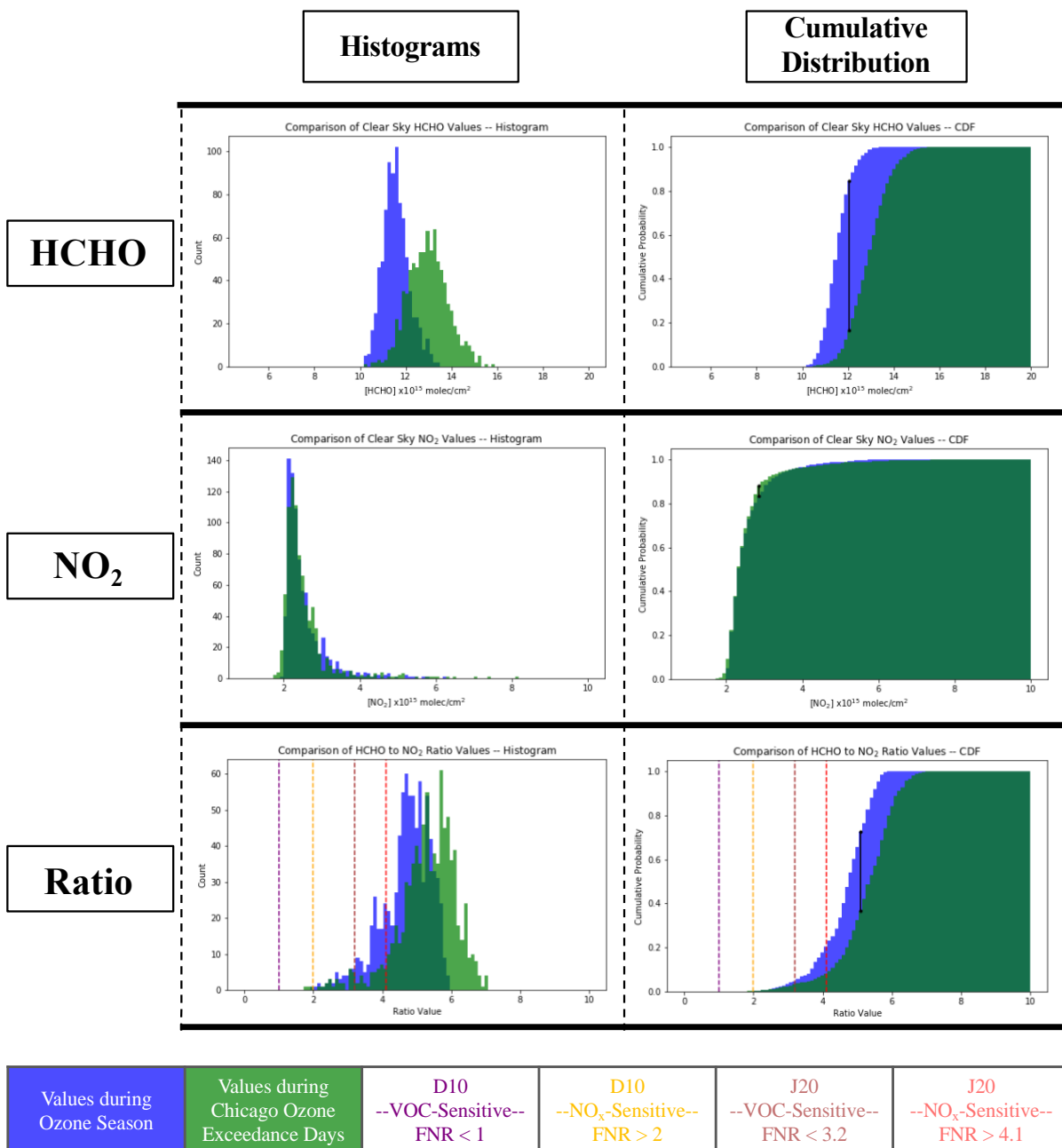
Figure 3.7 Histograms (left column) and CDFs (right column) of HCHO (top row), NO₂ (middle row), and FNR (bottom row) values for the combined 2018 and 2019 ozone seasons composite (blue) and for the ozone exceedance days within the Chicago NAA (green).

As seen in the histograms in **Figure 3.7**, there are shifts toward higher HCHO and FNR values during ozone exceedance days within the Chicago NAA. The results of the two-sample K-S tests show that these shifts are statistically significant. Because the result of the two-sample K-S test for NO_2 has a p-value greater than 0.05 (**Table 3.2**), NO_2 is not statistically different during ozone exceedance events versus the 2018-2019 ozone season. As a result, it is concluded that higher FNR values during ozone exceedance events are due to higher HCHO values. This behavior was similarly found in the results for each of the NAAs listed in **Section 2.2.2** (not shown).

If the results are interpreted using the D10 thresholds, it is important to note that while FNR values are shifted to higher values during ozone exceedance events, the actual values themselves suggest that the Lake Michigan region is dominated by NO_x-sensitive ozone production (FNR > 2) both during ozone exceedance events and during the typical ozone season. None of the values are below one, and a very small number of pixels (which are located within the Chicago Metropolitan Area) fall within the transition zone between NO_x-sensitive and VOC-sensitive ozone production (1< FNR < 2). However, interpreting the FNR values using the J20 thresholds tells a different and more nuanced story. During the typical ozone season, the CMA displays VOC sensitivity. Surrounding the CMA and north along the Wisconsin coast up to Milwaukee, the ratios suggest that ozone production falls in the transition zone. During Chicago ozone exceedance days, the CMA remains largely VOC-sensitive, and its surroundings are still in the transition zone, but the overall spatial extent of the transition zone decreases. North of the CMA along western Lake Michigan and up the Wisconsin coast to Milwaukee change to being more NO_x-sensitive during Chicago ozone

exceedance days. **Figure 3.8** visually demonstrates how the D10 and J20 thresholds lead to differing interpretations of ozone-NO_x-VOC sensitivity. This analysis shows that using the J20 thresholds for satellite data possibly reveals more insightful information about ozone production sensitivity in the Lake Michigan region.
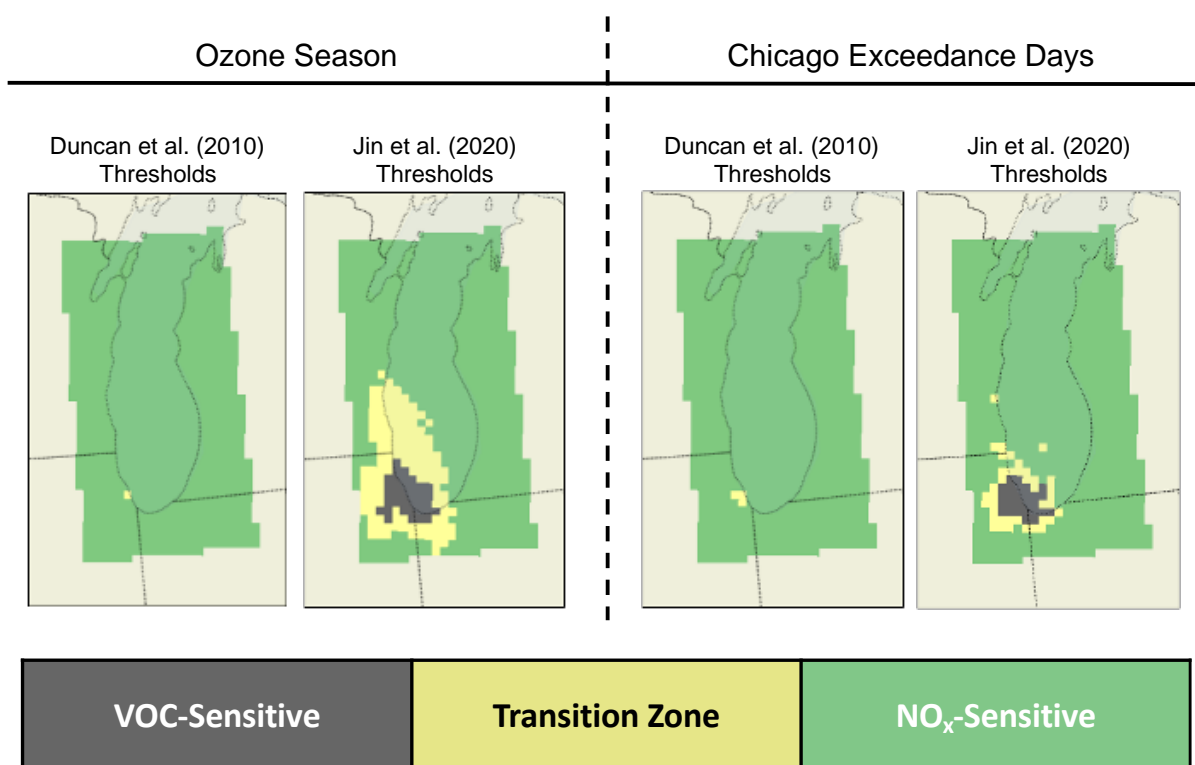
Figure 3.8 Classification of O_3 production regimes within the Lake Michigan region during the combined 2018-2019 O_3 seasons (left) and Chicago O_3 exceedance days (right).

3.4   EPA PAMS Ground FNRs & Comparisons to TROPOMI Satellite FNRs

For brevity, only results for EPA PAMS Site 3103 in Cook County, Illinois, (the only site within the Lake Michigan region) are discussed in this section. **Figure 3.9** shows time series plots of the calculated monthly mean FNRs at EPA PAMS Site 3103 in Cook County, Illinois, during the 2018 ozone season. Note that the two plots within the figure contain the same data points but have different ozone production sensitivity thresholds displayed. **Figure 3.9** reveals that the satellite FNRs are greater than ground FNRs for all months. The monthly mean ground FNRs ranged from a minimum of 0.08 in October to a maximum of 0.34 in July. In comparison, the monthly mean satellite ratio values ranged from a minimum of 1.42 in September to a maximum of 3.04 in June. There appears to be little, if any, correlation (r = 0.20) between the ground and satellite FNR values as they change from month-to-month. Similar results were found for the 2019 data at this site as well as for all the other sites of analysis (not shown), which answers the second research question of this study: monthly mean satellite-based TROPOMI FNRs are greater than monthly mean ground-based EPA PAMS FNRs.
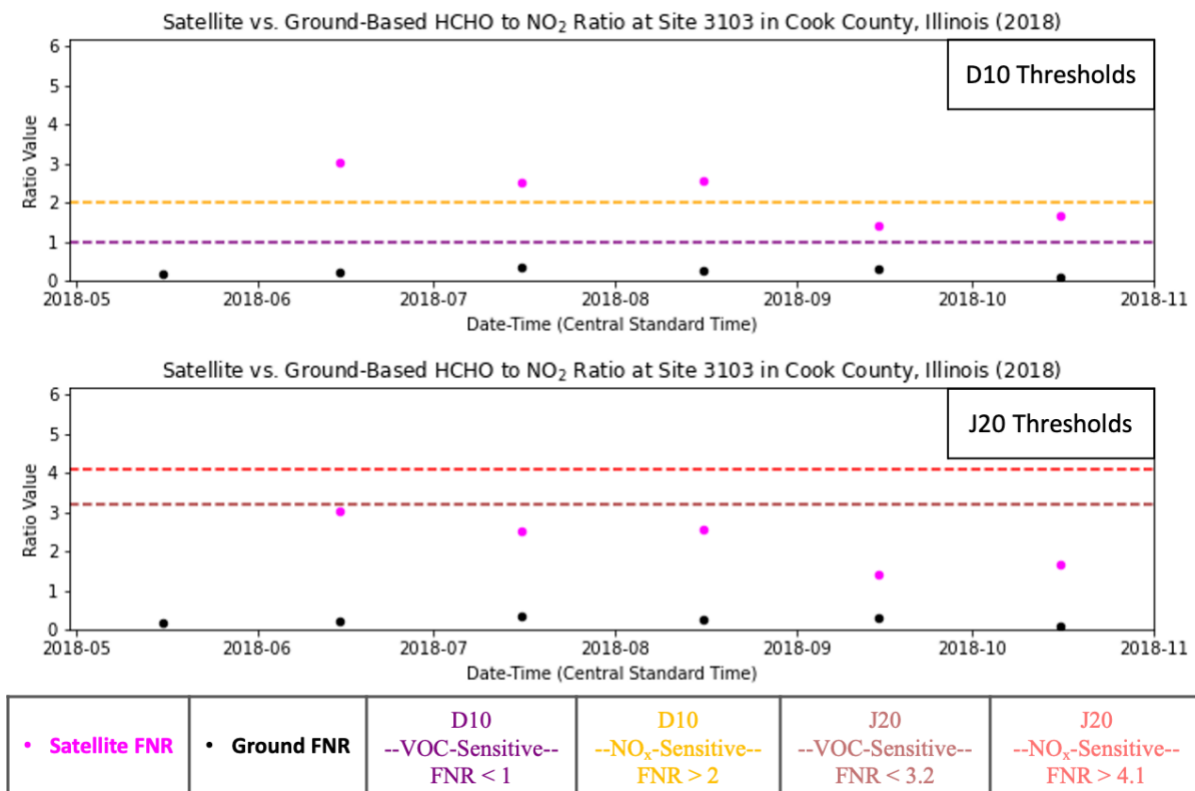
Figure 3.9 Time series plots of monthly mean ground and satellite FNRs for EPA PAMS Site 3103 in Cook County, Illinois, in 2018.

Furthermore, the differences between the ground and satellite data result in different interpretations of ozone production when applying the D10 thresholds to the FNR values. According to the ground FNRs, ozone production at this site is VOC-sensitive throughout the ozone season (FNR < 1) while the satellite ratios suggest that ozone production is NO_x-sensitive from June to August (FNR > 2) but in the transition zone in September and October (1 < FNR < 2). However, when using the J20 thresholds for satellite FNRs but the D10 thresholds for ground FNRs, interpretations of the ground-based and satellite-based ratios are congruent with one another. It should be noted that the J20 thresholds were not applied to the

ground FNRs because they were developed specifically for satellite data. The D10 thresholds were created using CMAQ and photochemical box modeling, which are known to simulate surface concentrations well; thus, it is assumed that they can be applied to ground FNRs. Using the D10 interpretation of ground FNRs and the J20 interpretation of the satellite FNRs suggests that this site is VOC-sensitive throughout the ozone season (**Table 3.3**). This congruence suggests that the D10 thresholds are more appropriate for interpreting surface measurements while the J20 thresholds are more appropriate for interpreting satellite data in the Lake Michigan region.

Table 3.3 Data values from Figure 3.9 and their interpretations of O_3 production sensitivity

Data Source	FNR/Threshold	June	July	Aug.	Sep.	Oct.
Ground	**FNR Value**	**0.23**	**0.34**	**0.26**	**0.31**	**0.08**
	D10 Interpretation	VOC	VOC	VOC	VOC	VOC
Satellite	**FNR Value**	**3.04**	**2.54**	**2.59**	**1.42**	**1.67**
	D10 Interpretation	NO_x	NO_x	NO_x	Transition	Transition
	J20 Interpretation	VOC	VOC	VOC	VOC	VOC

The large discrepancies in values between EPA PAMS ground FNRs and TROPOMI satellite FNRs leads to the third major question of this study, which is: what causes the differences between the two types of FNRs? There are two hypotheses for the causes of these differences that are explored in this study. The first hypothesis is that the 24-hour sampling of HCHO at EPA PAMS sites impacts the subsequent calculation of monthly mean FNRs because the HCHO concentration is not constant throughout the day. A 24-hour sample possibly 'dampens out' spikes in concentration that may occur in HCHO due to local industrial source emissions or sunlight-driven biogenic emissions, which can lead to decreased FNR values. The S5P satellite overpasses around 13:30 local solar time and TROPOMI captures instantaneous HCHO and NO_2 concentration values. Therefore, it would be more accurate to compare ground FNRs calculated from 1-hour measurement data to the TROPOMI FNRs, but the HCHO data at the EPA PAMS sites are limited to 8-hour or 24-hour samples. The second hypothesis, which was alluded to in **Section 1.3**, is that the vertical profiles of HCHO and NO_2 are different. EPA PAMS ground FNRs are calculated from boundary layer/surface concentrations while TROPOMI satellite FNRs are calculated from full tropospheric column concentrations. Differences in the vertical profiles of HCHO and NO_2 can therefore lead to differences between column (TROPOMI) FNRs and surface (EPA PAMS) FNRs. These two hypotheses are explored in the following sections.

3.5   LMOS 2017 Spaceport Sheboygan EPA Ground Site FNRs

To investigate the impact of 24-hour HCHO sampling on the calculation of monthly mean ground FNRs, high temporal 1-minute HCHO and NO_2 measurements collected during the LMOS 2017 field campaign at the Spaceport Sheboygan EPA ground site in Wisconsin were averaged into block intervals of 5 minutes, 1 hour, and 24 hours to represent different in situ sampling intervals (**Figure 3.10**). The block interval data were averaged again over the entire measurement period (~27 days) to get 'monthly' mean HCHO and 'monthly' mean NO_2 values, which were then divided to get 'monthly' mean FNRs for each block interval. **Table 3.4** shows that the FNR value decreases when the averaging interval for the data increases, but the differences are small. The monthly FNR of the raw 1-minute data is 0.693 while the monthly FNR of the 24-hour averaged data is 0.680, which are only about 2% different and still classified in the same ozone production regime. The methodology of first taking the monthly average of the HCHO and NO_2 data individually and then dividing the values to get a composite monthly FNR value makes it such that the averaging interval (representative of different sampling intervals) used on the data does not have a big impact on the calculated composite monthly FNR value. This analysis demonstrates that the 24-hour sampling of HCHO at EPA PAMS sites likely has a very small effect on the calculation of monthly mean ground FNR values from **Section 3.4** of this study.
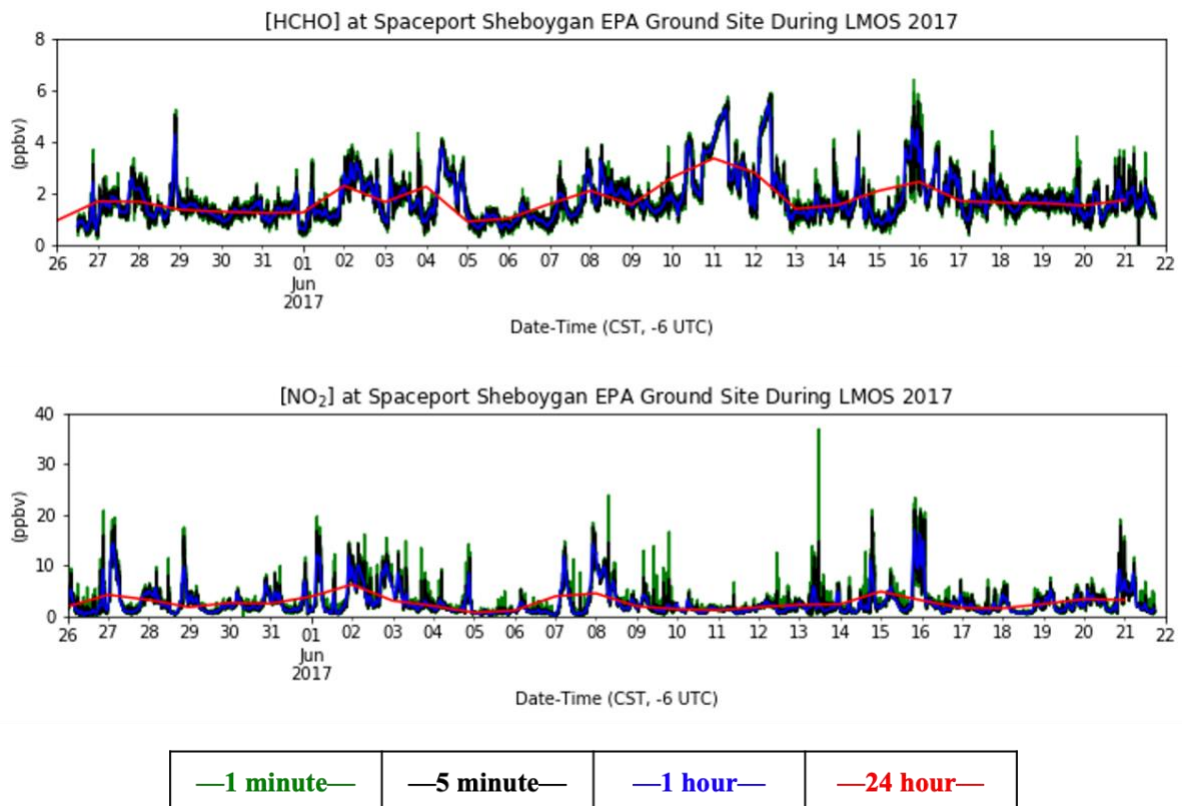
Figure 3.10 Time series plots of HCHO (top) and NO$_2$ (bottom) averaged into different time

block intervals at the Spaceport Sheboygan EPA ground site during LMOS 2017.

Table 3.4 Overall mean of data values in Figure 3.10 and the resulting FNR values

Averaging Interval	Mean HCHO ± 1 SD (ppb)	Mean NO$_2$ ± 1 SD (ppb)	FNR ± 1 SD* (Mean HCHO / Mean NO$_2$)
1-minute (raw)	1.787 ± 0.895	2.579 ± 2.686	0.693 ± 0.714
5-minute	1.772 ± 0.878	2.580 ± 2.647	0.687 ± 0.694
1-hour	1.771 ± 0.839	2.588 ± 2.475	0.684 ± 0.648
24-hour	1.756 ± 0.571	2.580 ± 1.236	0.680 ± 0.372

*Note: The standard deviations (SD) of the FNR values were approximated using equation

(20) from Steltman (2018).

Although the methodology of this study leads to monthly mean FNR values that are not greatly impacted by the 24-hour sampling of HCHO, the concentrations of HCHO and NO_2 are not well represented by long-term (e.g., 24-hour) in situ samples. The time series of the raw 1-minute data in **Figure 3.10** shows that HCHO and NO_2 concentrations varied throughout individual days at the Spaceport Sheboygan EPA ground site during LMOS 2017. Furthermore, when looking at the differently averaged interval data (representative of different in situ sampling intervals), **Figure 3.10** indicates that as the averaging interval increases, the calculated HCHO and NO_2 can decrease, 'dampening out' any spikes in concentration. For example, on June 16, 2017, at 0:00 local time, the HCHO 1-minute raw and 5-minute averaged data suggest a concentration of ~6 ppb, but the 1-hour averaged data suggests ~4 ppb and the 24-hour averaged data suggests ~2 ppb. Similarly, on June 8, 2017, at 0:00 local time, the NO_2 1-minute raw, 5-minute averaged, and 1-hour averaged data suggest a concentration of ~20 ppb, but the 24-hour averaged data suggests ~5 ppb. This 'dampening effect' is also seen in the monthly composited HCHO and NO_2 data in **Table 3.4**, which shows that as the averaging interval increases, the standard deviation decreases. In other words, the variability in HCHO concentrations indicated by the larger standard deviation value of the raw 1-minute data is not represented well by the smaller standard deviation of the 24-hour averaged data, proving that the 24-hour sampling of HCHO at EPA PAMS sites is not representative of the fluctuations in the atmospheric abundance of this gas throughout the day.

The fact that HCHO and NO_2 concentrations vary throughout the day means that ozone production sensitivity, and thus FNR values, can also vary throughout the day. This nuance is not captured in the composite monthly mean ground FNR values calculated from 24-hour

samples of HCHO measured at EPA PAMS sites. To illustrate this point, **Figure 3.11** shows a time series of 'instantaneously' calculated FNR values from the differently averaged data in **Figure 3.10**. On May 28, 2017, the FNR values calculated from the raw 1-minute data cycle between a minimum of ~0.5 and a maximum of ~3, indicating that ozone production cycles between VOC and NO_x sensitivity. On the same day, the FNR value of the 24-hour averaged data is ~0.6, which indicates VOC-sensitivity. This singular datapoint does not show how ozone production changes throughout the day. Furthermore, as the time-averaging interval increases (representing increasingly longer in situ sampling intervals), the calculated FNR value typically decreases. For example, on June 18, 2017, the raw 1-minute data has an FNR value of ~4 while the 24-hour averaged data has an FNR value of ~0.95. This leads to different interpretations of ozone production sensitivity, with the raw data indicating NO_x sensitivity but the 24-hour averaged data indicating VOC sensitivity.
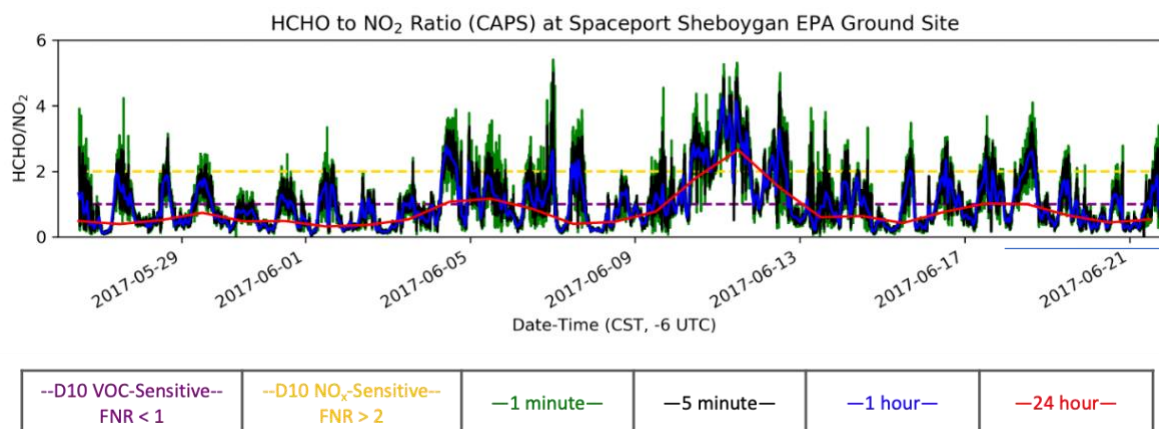
Figure 3.11 Time series plot of 'instantaneous' FNR values calculated in differing averaging intervals at the Spaceport Sheboygan EPA ground site during LMOS 2017.

Table 3.5 shows 'monthly' mean FNR values for each time interval calculated by taking the average of the 'instantaneous' FNR values throughout the entire time series in **Figure 3.11**. Again, this demonstrates that as the averaging interval increases, the resulting 'monthly' mean FNR value decreases. However, the decrease is much larger (~30%) than when monthly mean NO_2 and HCHO concentrations are used to calculate 'monthly' mean FNR values. The 24-hour averaged 'monthly' mean FNR value of 0.783 indicates a different ozone production regime than the 1-minute 'monthly' mean FNR value of 1.124, indicating VOC sensitivity and the transition zone, respectively. This shows how long term (e.g., 24-hour) sampling of HCHO at EPA PAMS sites can lead to incorrect interpretations of ozone production sensitivity.

Table 3.5 'Monthly' mean FNR values for the different time-averaged data in Figure 3.11

Averaging Interval	'Monthly' Mean FNR ± 1 SD
1-minute (raw)	1.124 ± 0.841
5-minute	1.089 ± 0.800
1-hour	1.026 ± 0.748
24-hour	0.783 ± 0.520

Another way to investigate the impact of 24-hour HCHO sampling on FNR values is to look at the average diurnal cycles of HCHO, NO_2, and FNR values at the Spaceport Sheboygan EPA ground site during LMOS 2017 (**Figure 3.12**). At Spaceport Sheboygan during LMOS 2017, the average HCHO diurnal cycle (top plot of **Figure 3.12**) shows two peaks in concentration at 8:00 am and 8:00 pm local time, while the lowest concentrations occur at 1:00 am and 3:00 pm local time, dropping approximately 30% from the peak concentrations. Interestingly, the average HCHO diurnal cycle at Spaceport Sheboygan during LMOS 2017 has a different pattern than that found in other studies. For example, Franco et al. (2016) derived HCHO total columns from ground-based high-resolution Fourier transform infrared solar spectra recorded at a rural, high-altitude station in the Swiss Alps. They found a general HCHO diurnal cycle in which HCHO levels increase in the morning hours, peak around noon local time, gradually decrease in the afternoon, and drop off at night. The Franco et al. (2016) singularly peaked HCHO diurnal cycle is different than the Spaceport Sheboygan HCHO diurnal cycle presented here likely because they used a remote sensing technique to approximate column measurements at a rural site where biogenic HCHO concentrations are driven by the diurnal cycle in solar insolation. At Spaceport Sheboygan, measurements were made in situ and on the surface, which are affected by biogenic and potential local sources as well as the transport of anthropogenic sources of HCHO. A study by Li et al. (2014) used long-path differential optical absorption spectroscopy (DOAS) to measure HCHO in urban Shanghai, China, and found an average diurnal cycle that was doubly peaked around 10:00 am and 4:00 pm local time, with concentrations generally higher during that day than at night. The Li et al. (2014) findings are more similar to the Spaceport Sheboygan HCHO diurnal cycle

because their measurement site was in an urban setting, and the DOAS methodology is closer to the in situ Spaceport Sheboygan surface measurements than the method used by Franco et al. (2016). However, the differences in the times of occurrence of the peaks within the diurnal cycle indicate that in urban settings, local sources of HCHO and transport of anthropogenic HCHO impact the diurnal cycle in addition to sunlight driven biogenic HCHO emissions. The average NO_2 diurnal cycle at Spaceport Sheboygan during LMOS 2017 (middle plot of **Figure 3.12**) has higher concentrations at night than during the day. This cycle follows a similar pattern, but shifted in time, as that for the Chicago Metropolitan Area found by Wang et al. (2020). Again, the dissimilarities in Wang et al. (2020) and Spaceport Sheboygan diurnal cycles could be due to differences in local source emissions of NO_2 (e.g., differences in traffic volumes and thus car exhaust emissions of NO_2). As seen in the bottom plot of **Figure 3.12**, the average diurnal cycle of FNR values indicates that ozone production starts off as VOC-sensitive in the early morning hours, becomes more NO_x-sensitive during the day, and returns to being VOC-sensitive at night. These plots show that the diurnal cycles of HCHO and NO_2 result in time varying FNR values that indicate different ozone production regimes throughout the day.
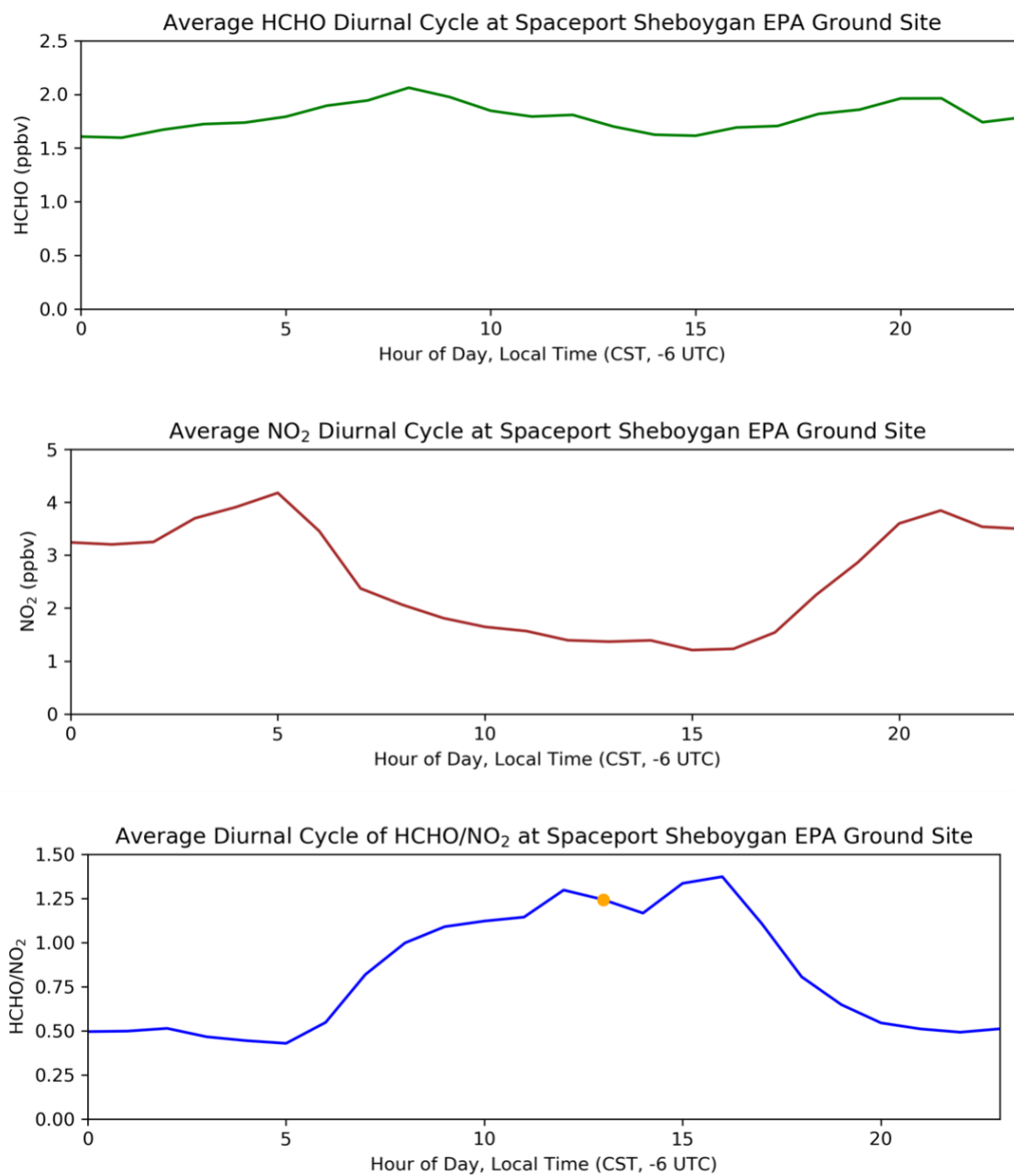
Figure 3.12 Plots of the average diurnal cycles of HCHO (top), NO₂ (middle), and the
resulting FNR values (bottom) at the Spaceport Sheboygan EPA ground site during LMOS
2017.

The diurnal cycles of HCHO and NO_2 also partially explain why there are discrepancies in the TROPOMI satellite FNR values and EPA PAMS ground FNR values presented in **Section 3.4**. In the bottom plot of **Figure 3.12**, the orange marker indicates that the FNR value of the 1:00 pm (13:00) local time datapoints is ~1.24; this more closely resembles what TROPOMI would instantaneously observe during the S5P satellite overpass time. Meanwhile, the monthly average of all the raw 1-minute data for HCHO and NO_2 during the sampling period leads to a 'monthly' FNR value of ~0.69 (1.8 times smaller than the 1:00 pm FNR); this more closely resembles what was calculated from the EPA PAMS data in this study. Instantaneous TROPOMI retrievals capture HCHO and NO_2 concentrations at a specific time within their diurnal cycles. The 24-hour sampling of HCHO at EPA PAMS sites captures an average of the concentrations within the HCHO diurnal cycle, which is often different than the 1:00 pm concentration. This can lead to differences between ground FNR values calculated from EPA PAMS data and satellite FNRs calculated from TROPOMI data.

These analyses bring up an important point about the limitations of the methodology used in this and other similar studies. Because of the lower signal-to-noise ratios of HCHO retrievals from satellite instruments, the data had to be averaged into monthly composites. Subsequent calculations of FNR values from the satellite data only allows for the interpretation of the average ozone production sensitivity for a region for that specific month during the satellite overpass time. However, the raw 1-minute data in **Figure 3.11** shows that there is a diurnal variation in FNR values and ozone production regimes between VOC and NO_x sensitivities, which is driven by the diurnal cycles of HCHO and NO_2 seen in **Figures 3.10 and 3.12**. While knowing the 'typical' ozone production sensitivity regime that an airshed falls into

is a useful piece of information for air quality regulatory agencies, such information obscures the short-term variations in ozone production sensitivity that would need to be considered to fully address ozone air pollution problems.

3.6   **LMOS 2017 CMAQ Simulations: HCHO and NO_2 Vertical Profiles**

To test the second hypothesis for the causes of the discrepancies between TROPOMI and EPA PAMS FNRs, vertical profiles of HCHO and NO_2 above Spaceport Sheboygan, Wisconsin, were compared using LMOS 2017 CMAQ simulation data. Before looking at the vertical profiles, surface measurements from the Spaceport Sheboygan EPA ground site were compared to surface concentrations within the model output to evaluate model simulation accuracy (**Figure 3.13**). Model and in situ HCHO have a correlation of 0.66, bias of -0.26 ppb, and root mean square error (RMSE) of 0.74 ppb. Model and in situ NO_2 have a correlation of 0.42, bias of 0.68 ppb, and RMSE of 2.87 ppb. While the model does not perfectly simulate the in situ measurements, the plots demonstrate that the same general patterns in concentrations exist within both datasets. Therefore, it appears reasonable to evaluate near surface HCHO and NO_2 vertical profiles from the CMAQ simulations.
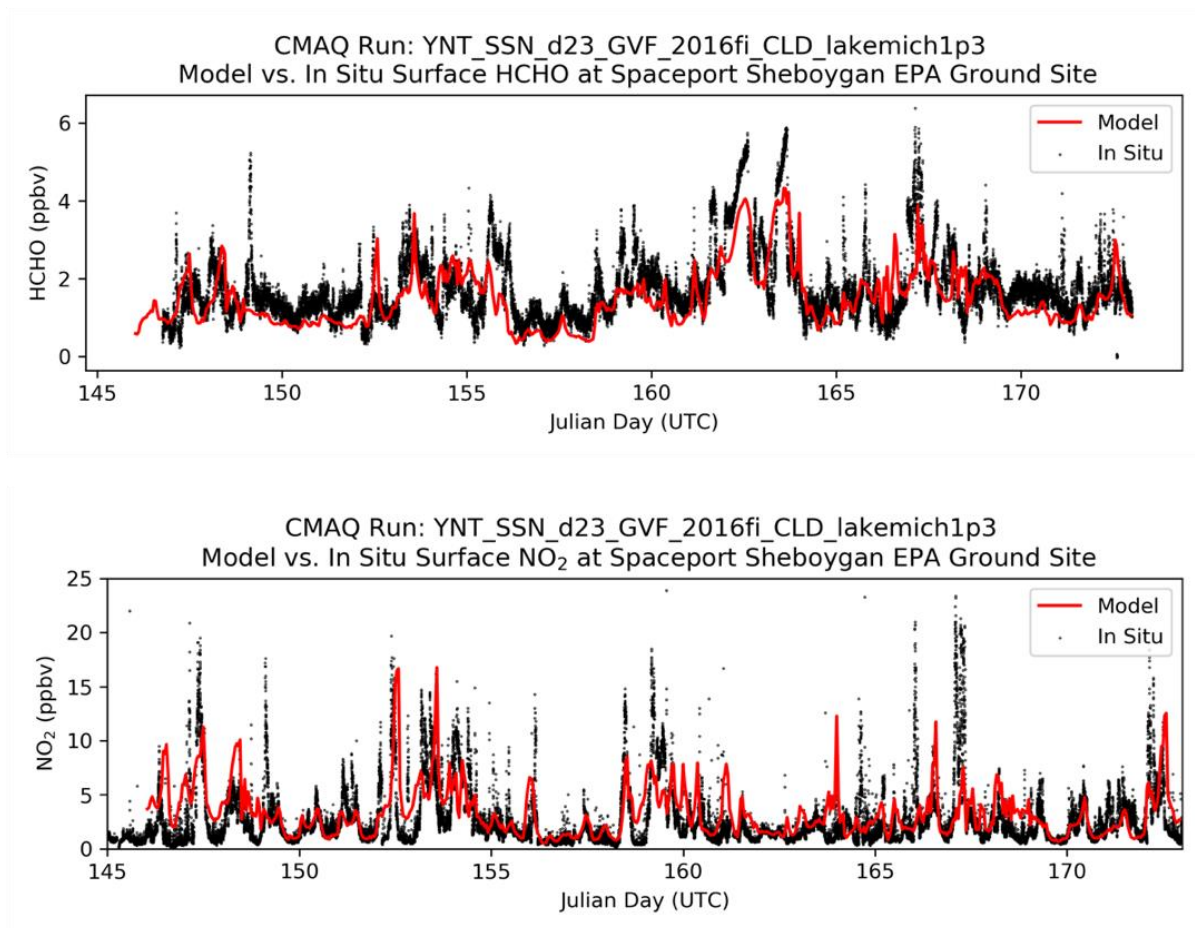
Figure 3.13 Comparisons of in situ and model surface HCHO (top) and NO₂ (bottom) at the

Spaceport Sheboygan EPA ground site during LMOS 2017.

Figure 3.14 shows the CMAQ vertical profiles up to an altitude of 3 km for HCHO and NO_2 over Spaceport Sheboygan. Clearly, there are profile differences between HCHO and NO_2. In general, it appears that HCHO typically extends further up at higher concentrations in the atmosphere than NO_2 (particularly above altitudes of 1 km) and is generally monotonic with altitude. In contrast, NO_2 concentrations are much greater near the surface (below altitudes of 0.5 km) and are often not monotonic with altitude. The regions denoted with a red box show an example of where HCHO extends much further up in the atmosphere than NO_2.
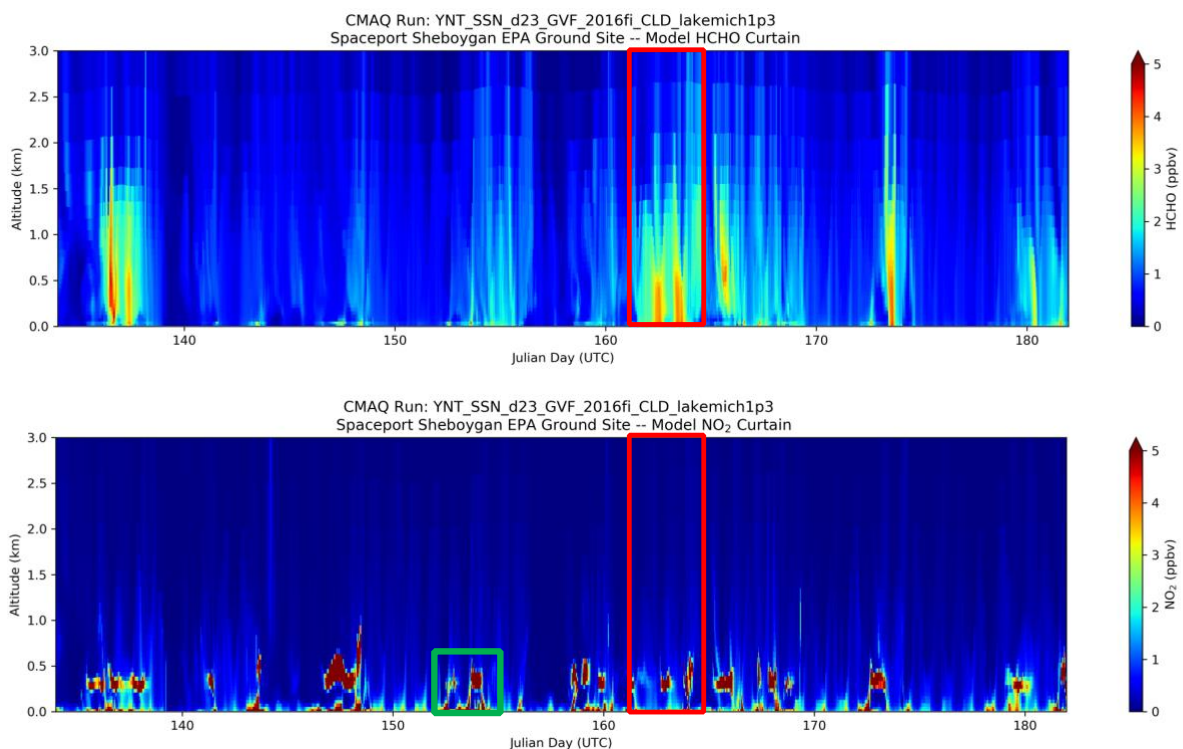
Figure 3.14 CMAQ vertical profiles of HCHO (top) and NO_2 (bottom) over the Spaceport Sheboygan EPA ground site. The red and green boxed regions are discussed in the main text.

Figure 3.15 displays a time series that compares the surface FNR to the 0-3.2 km column FNR over Spaceport Sheboygan within the CMAQ simulations. The 0-3.2 km column FNR is greater than the surface FNR over 99% of the time, with an average difference (column FNR – surface FNR) of 2.15. When looking at **Figures 3.14** and **3.15** together, it appears that the largest differences between column and surface FNR values occur when either: (1) NO_2 and HCHO both have low concentrations throughout the column, or (2) NO_2 has low concentrations but HCHO has elevated concentrations throughout the column. Another insight gained from **Figure 3.15** is that the variability of the 0-3.2 km column FNR values (standard deviation ~ 1.69) is larger than that of the surface FNR values (standard deviation ~ 0.42). The larger variability of the column FNR values is possibly due to the intrusion of HCHO higher into the atmosphere as well as the lofted NO_2 features around 0.5 km altitude, which are discussed further in **Section 3.7**. Although there are large numerical differences between the surface and column FNRs within the simulations, the time series have a moderately strong positive linear relationship as indicated by a correlation coefficient (r) value of about +0.60. Together, the analyses of **Figures 3.14** and **3.15** provide an answer to the third major research question of this study, which is that profile differences in HCHO and NO_2 can cause discrepancies between column (TROPOMI) and surface (EPA PAMS) FNR values. In particular, HCHO often reaches up higher into the atmosphere than NO_2, resulting in column FNRs greater than surface FNRs.
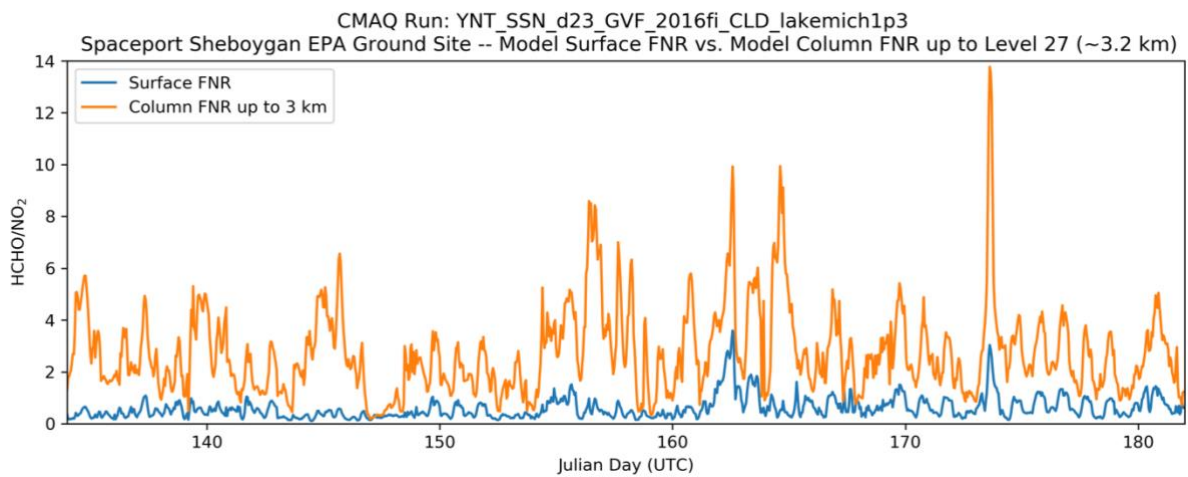
Figure 3.15 Comparison of CMAQ surface FNRs and 0-3.2 km vertical column FNRs over

the Spaceport Sheboygan EPA ground site.

3.7 Scientific Aviation NO$_2$ Profiles & Comparisons to CMAQ Output

Also seen in **Figure 3.14** are lofted NO$_2$ features, such as those within the green box region in the bottom plot. Since these features are above the surface, they can also cause discrepancies between total column FNRs and surface FNRs. To see if these CMAQ-simulated lofted features are real, CMAQ output was compared to Scientific Aviation in situ flight measurements of NO$_2$ from June 2, 2017, in **Figure 3.16**. As the plane spiraled up and down above Spaceport Sheboygan, the in situ measurements show elevated NO$_2$ concentrations between 0.4 and 0.6 km. This confirms that the lofted NO$_2$ features seen in **Figure 3.14** are real and that the model may be underestimating their concentrations. Further investigation of the CMAQ simulations suggest that the plumes observed at the Spaceport Sheboygan EPA ground site originated at the Edgewater Coal Plant, which emits NO$_2$ from a tall smokestack. As the NO$_2$ emitted from the smokestack is transported by wind, the locations where the lofted NO$_2$ travels can cause a disconnect between surface and total column FNRs.
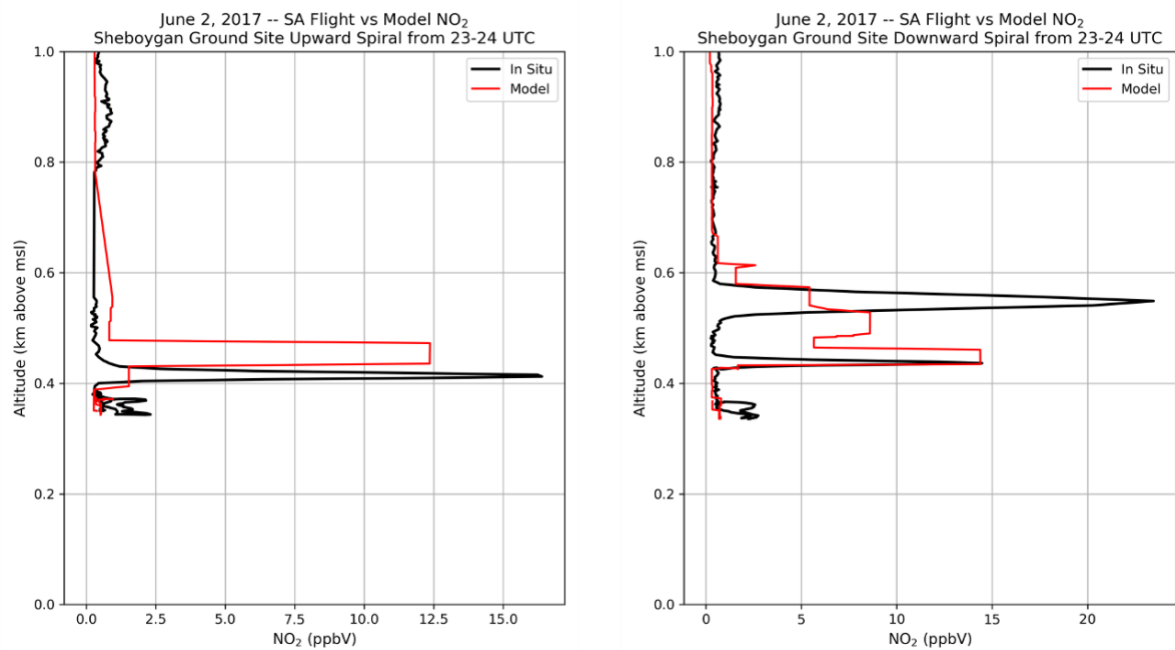
Figure 3.16 Comparisons between CMAQ simulations and in situ flight measurements of

NO₂ over Spaceport Sheboygan on June 2, 2017.

3.8   Limitations, Assumptions, & Suggestions for Future Work

There are a few limitations and assumptions in this study that need to be discussed to provide full context to the results presented. First, it was assumed that the thresholds for ozone-NO_x-VOC sensitivity determined by D10 and J20 for OMI data can be applied to TROPOMI data because of the similarities in SNRs. However, the two instruments have very different spatial resolutions, which could impact the thresholds for ozone-NOx-VOC sensitivity if determined solely using TROPOMI data. Similarly, the detection limit filters used when creating the TROPOMI composites are also for OMI data, but the true detection limits of TROPOMI for HCHO and NO_2 may be different. Third, the EPA PAMS ground FNR data in **Section 3.4** and **Table 3.3** were interpreted using the D10 thresholds. While the D10 thresholds were meant to be applied to satellite data by Duncan et al. (2010), it is assumed in this work that they are applicable to in situ surface data since the thresholds were determined using CMAQ and photochemical box modeling, which are known to simulate surface concentrations well. This assumption, however, may not be completely accurate. Furthermore, the D10 thresholds are not necessarily geographically specific. The true FNR threshold value between VOC-sensitive and NO_x-sensitive ozone production can vary from airshed to airshed, so the D10 thresholds maybe different than what is truly correct for the Lake Michigan region.

LMOS 2017 CMAQ simulations were compared to surface HCHO and NO_2 observations and airborne in situ NO_2 measurements, which showed acceptable agreement between the model and in situ data. Unfortunately, there were no in situ vertical profiles of HCHO measured from the Scientific Aviation flights during LMOS 2017. Such data would have provided additional evidence to support the finding within the CMAQ curtain plots

(**Figure 3.14**) that HCHO extends further up into the atmosphere than NO_2. The CMAQ simulations used in this work also bring up other aspects of FNRs that are potentially worth exploring. For example, HCHO yield is dependent on the source of VOC (e.g., biogenic versus anthropogenic VOC emissions). One could perform sensitivity experiments within CMAQ to evaluate whether perturbing biogenic or anthropogenic VOC emissions has a greater effect on the resulting FNR values. Another possible line of inquiry would be to dive further into the relationship between surface and column FNR values, specifically outside of NO_x and anthropogenic HCHO source regions. One could sample various geographical locations within the CMAQ simulations used in this study to see if the relationship between surface and column FNRs are different for urban city centers, rural sites downwind of urban areas, isolated rural areas, etc.

Last, as was discussed in **Section 3.5**, the creation of monthly mean FNRs from satellite data obscures the diurnal cycle in FNR values and ozone production sensitivity seen in **Figures 3.11 and 3.12**, which can prove to be a big limitation for air quality management agencies that create policy to address ozone air quality issues in their region. In all, calculating ozone-NO_x-VOC sensitivity thresholds using the J20 methodology with TROPOMI data, determining the actual detection limits of TROPOMI HCHO and NO_2 retrievals, and establishing the true ozone-NO_x-VOC sensitivity thresholds using ground data within the Lake Michigan region airshed are suggestions for future work that could build upon this thesis research. Additionally, having more continuous VOC measurements at EPA PAMS sites, higher precision HCHO satellite retrievals, and higher temporal resolution satellite retrievals of HCHO and NO_2 would

greatly improve future research studies that utilize the FNR to indicate ozone production sensitivity.

CHAPTER 4: SUMMARY & CONCLUSIONS

This study investigated the formaldehyde to nitrogen dioxide ratio ('FNR') using satellite, in situ, and air quality modeling data. The first and second parts of this work explored the use of satellite-based FNRs as an indicator of ozone-NO_x-VOC sensitivity in the Lake Michigan region. The satellite FNR values were interpreted using two different sets of thresholds for ozone production sensitivity, one from Duncan et al. (2010) ('D10') and one from Jin et al. (2020) ('J20'). In general, the results of this study showed that the J20 thresholds are more appropriate for interpreting the TROPOMI satellite FNRs and the D10 thresholds are more appropriate for interpreting the EPA PAMS surface FNRs presented in this work.

The results also demonstrated that binning satellite data onto a 12 x 12 km^2 grid allows one to see the spatial distribution of atmospheric NO_2 and HCHO on a monthly basis. Because TROPOMI retrievals of HCHO are noisier than NO_2, the data needed to be composited into monthly averages to reduce the influence of noise in the HCHO retrievals. Results for the 2018 and 2019 ozone seasons showed that the minimum FNRs occurred over NYC (1.64) and Chicago (1.92), which places both urban centers in VOC-sensitive regimes based on J20 thresholds. Monthly composite results showed that in the Lake Michigan region, the Chicago Metropolitan Area (CMA) is VOC-sensitive, its surroundings and north along the Wisconsin shoreline up to Milwaukee are in the transition zone, and the rest of the region falls within the NO_x-sensitive ozone production regime based on the J20 thresholds. These results are similar to those of Vermeuel et al. (2019), who used chemical box modeling to investigate the ozone production sensitivity of an air parcel as it traveled on June 2, 2017, from its Chicago-Gary

urban source region to over Lake Michigan, and then north along the coast to the receptor site of Zion, Illinois. Their findings show that ozone production within the plume was strongly VOC-sensitive in its Chicago-Gary urban source region and became more NO_x-sensitive as it advected north along the Lake Michigan coastline. Both this study and that of Vermeuel et al. (2019) found a general south-north gradient in ozone production regimes that transitions toward less VOC sensitivity/more NO_x sensitivity starting from the south in the Chicago Metropolitan Area and going north along the Lake Michigan shoreline.

TROPOMI FNR composites interpreted using the J20 thresholds suggest that during the ozone season and during Chicago ozone exceedance events, the CMA remains VOC-sensitive, but the spatial extent of the transition zone that surrounds Chicago and extends north up to Milwaukee decreases during ozone exceedance events (FNR values increase). Statistical tests show that the higher FNR values are due to higher background HCHO levels rather than changes in NO_2. This is likely attributed to increased temperatures during ozone exceedance events, which leads to increased biogenic VOC emissions and thus increased ozone production (Sillman & Samson, 1995). Future work could investigate this hypothesis via performing perturbation CMAQ simulations to determine if it is increases in biogenic or anthropogenic VOC emissions that are responsible for higher FNR values and changes in ozone production sensitivity during ozone exceedance days.

In the third part of this work, comparisons between ground-based EPA PAMS and satellite-based TROPOMI FNR values revealed large numerical differences, with the monthly satellite ratios always being greater than the monthly ground ratios. In the final part of this research, reasons for the disconnect between the two types of FNRs were explored. The first

hypothesis, which is that the lower temporal resolution of HCHO measurements (24-hour samples) at EPA PAMS sites affects the calculation of monthly mean FNR values, was tested through analysis of high temporal resolution HCHO and NO_2 measurements collected during LMOS 2017 at the Spaceport Sheboygan EPA ground site. The 'monthly' average FNR of the raw 1-minute data was 0.69 while the 'monthly' average FNR of the 24-hour averaged data was 0.68. These analyses show that because the EPA PAMS FNRs were calculated by first averaging the HCHO and NO_2 data on a month-by-month basis and then dividing the monthly averages to get a monthly FNR value, longer term sampling has little to no effect on the ground FNR values presented in **Section 3.4** of this study.

Although the monthly mean FNR values in **Section 3.4** were not impacted by the 24-hour sampling of HCHO, analysis of the high-resolution LMOS 2017 measurements revealed major limitations of the methodology of this work as well as the low temporal resolution HCHO sampling at EPA PAMS sites. Time series of the LMOS 2017 HCHO and NO_2 data demonstrated that both gases have concentrations that follow unique diurnal cycles, which means that FNR values (and thus ozone production sensitivity) also change throughout the day. Such intraday shifts between VOC-sensitive and NO_x-sensitive ozone production are not captured by monthly mean FNR values. The existence of the HCHO diurnal cycle also means that the 24-hour sampling of HCHO at EPA PAMS sites can 'dampen' out spikes in concentrations seen throughout the day. Plots of the average diurnal cycles of HCHO and NO_2 at Spaceport Sheboygan during LMOS 2017 showed that the FNR value of the 1:00 pm local time datapoints is 1.24 (which resembles what TROPOMI would see as it overpasses), while the average of all the raw 1-minute data gives an FNR value of 0.69 (which resembles what

was calculated from the EPA PAMS data in this study). Therefore, low temporal resolution sampling of HCHO at EPA PAMS sites impact the calculation of 'instantaneous' FNRs and can lead to incorrect interpretations of ozone production sensitivity.

The second hypothesis that was explored (for the differences between TROPOMI and EPA PAMS FNR values) is that the differences in the vertical profiles of HCHO and NO_2 can lead to different surface and column FNR values. Analysis of LMOS 2017 CMAQ simulations showed that HCHO often extends further up into the atmosphere than NO_2, causing column FNRs to have greater values than surface FNRs. Despite these numerical differences, a statistical comparison of CMAQ surface and 0-3.2 km column FNR time series revealed that the two have a moderately strong positive linear relationship as indicated by a correlation coefficient (r) value of about +0.60. It was also shown that lofted NO_2 plumes from tall point sources (such as coal-fired power plants) cause further differences between surface and column ratios. Testing this second hypothesis demonstrated that ratios of satellite column measurements of HCHO and NO_2 do not necessarily reflect the ratios of surface measurements.

Based on the results of this study, it is concluded that satellite-based TROPOMI FNRs and ground-based EPA PAMS FNRs require different thresholds for NO_x versus VOC sensitivities. Using the J20 thresholds to interpret satellite ratios and using the D10 thresholds to interpret surface ratios led to consistent interpretations of ozone-NO_x-VOC sensitivity in the Lake Michigan region. However, due to sampling interval limitations at many EPA PAMS sites, only 8-hour or 24-hour HCHO samples are collected, which leads to FNRs calculated from such data that are often lower than instantaneously calculated ratios because of the diurnal cycles of HCHO and NO_2. It would be more accurate to compare in situ ground measurements

taken at 13:00 local solar time to the TROPOMI data since that is the S5P overpass time. Even then, vertical profile differences between HCHO and NO_2 makes direct comparisons between satellite and ground FNRs difficult. This highlights the need for more consistent and higher temporal resolution VOC measurements at EPA PAMS sites as well as higher precision HCHO and higher temporal resolution HCHO and NO_2 satellite retrievals. The NASA Tropospheric Emissions: Monitoring of Pollution (TEMPO) mission will launch a geostationary-orbiting satellite into space in 2022 carrying a visible and ultraviolet light grating spectrometer that is capable of measuring air pollutants, including HCHO and NO_2, in hourly intervals over the United States (Zoogman et al., 2017). Such measurements represent a significant advancement in the field of atmospheric chemistry and will provide researchers with more datasets to explore how information from satellite-based formaldehyde to nitrogen dioxide ratios can be utilized to properly address ozone air pollution problems throughout the country.

REFERENCES

Abdioskouei, M., Adelman, Z., Al-Saadi, J., Bertram, T., Carmichael, G., Christiansen, M.,

    … Wagner, T. (2019). 2017 *Lake Michigan Ozone Study (LMOS) preliminary finding*

    report. Lake Michigan Air Directors Consortium. Retrieved May 7, 2021, from

    https://www.ladco.org/wp-

    content/uploads/Research/LMOS2017/LMOS_LADCO_report_revision_apr2019_fin

    al.pdf

Anenberg, S. C., West, J. J., Fiore, A. M., Jaffe, D. A., Prather, M. J., … Zeng, G. (2009).

    Intercontinental impacts of ozone pollution on human mortality. *Environmental*

    Science & Technology, 43(17), 6482-6487. https://doi.org/10.1021/es900518z

Avnery, S., Mauzerall, D. L., Liu, J., & Horowitz, L. W. (2011). Global crop yield reductions

    due to surface ozone exposure: 1. Year 2000 crop production losses and economic

    damage. *Atmospheric Environment, 45*(13), 2284-2296.

    https://doi.org/10.1016/j.atmosenv.2010.11.045

Chance, K. (Ed.). (2002). *OMI algorithm theoretical basis document, volume IV, OMI trace*

    gas algorithms. Smithsonian Astrophysical Observatory & National Aeronautics and

    Space Administration. Retrieved May 7, 2021, from

    https://ozoneaq.gsfc.nasa.gov/media/docs/ATBD-OMI-04.pdf

Chang, C. Y., Faust, E., Hou, X., Lee, P., Kim, H. C., Hedquist, B. C., & Liao, K. J. (2016).

    Investigating ambient ozone formation regimes in neighboring cities of shale plays in

    the Northeast United States using photochemical modeling and satellite retrievals.

Atmospheric Environment, 142, 152-170.

https://doi.org/10.1016/j.atmosenv.2016.06.058

De Smedt, I., Romahn, F., Eichmann, K.-U., Lambert, J.-C., Loyola, D., Veefkind, J. P., Dehn, A., & Zehner, C. (2020, July 16). *S5P mission performance centre formaldehyde [L2__HCHO___] readme*. European Space Agency. Retrieved May 7, 2021, from http://www.tropomi.eu/sites/default/files/files/publicSentinel-5P-Formaldehyde-Readme.pdf

De Smedt, I., Theys, N., Yu, H., Danckaert, T., Lerot, C., Compernolle, S., … Veefkind, P. (2018). Algorithm theoretical baseline for formaldehyde retrievals from S5P TROPOMI and from the QA4ECV project. *Atmospheric Measurement Techniques, 11*(4), 2395-2426. https://doi.org/10.5194/amt-11-2395-2018

Duncan, B. N., Yoshida, Y., Olson, J. R., Sillman, S., Martin, R. V., Lamsal, L., … Crawford, J. H. (2010). Application of OMI observations to a space-based indicator of NO$_x$ and VOC controls on surface ozone formation. *Atmospheric Environment, 44*(18), 2213-2223. https://doi.org/10.1016/j.atmosenv.2010.03.010

Ek, M. B., Mitchell, K. E., Lin, Y., Rogers, E., Grunmann, P., Koren, V., … Tarpley, J. D. (2003). Implementation of Noah land surface model advances in the National Centers for Environmental Prediction operational mesoscale Eta model. *Journal of Geophysical Research: Atmospheres, 108*(D22), 8851. https://doi.org/10.1029/2002JD003296

Eskes, H. J., Eichmann, K.-U., Lambert, J.-C., Loyola, D., Veefkind, J. P., Dehn, A., & Zehner, C. (2020, November 26). *S5P mission performance centre nitrogen dioxide*

[L2__NO2___] readme. European Space Agency. Retrieved May 7, 2021, from

https://sentinel.esa.int/documents/247904/3541451/Sentinel-5P-Nitrogen-Dioxide-

Level-2-Product-Readme-File

Franco, B., Marais, E. A., Bovy, B., Bader, W., Lejeune, B., Roland, G., … Mahieu, E.

(2016). Diurnal cycle and multi-decadal trend of formaldehyde in the remote

atmosphere near 46ºN. *Atmospheric Chemistry and Physics, 16*(6), 4171-4189.

https://doi.org/10.5194/acp-16-4171-2016

Geffen, J. v., Boersma, K. F., Eskes, H., Sneep, M., Linden M. t., Zara, M., & Veefkind, J. P.

(2020). S5P TROPOMI NO_2 slant column retrieval: method, stability, uncertainties

and comparisons with OMI. *Atmospheric Measurement Techniques, 13*(3), 1315-

1335. https://doi.org/10.5194/amt-13-1315-2020

Geffen, J. v., Eskes, H., Boersma, K. F., Maasakkers, J. D., & Veefkind, J. P. (2019).

TROPOMI ATBD of the total and tropospheric NO_2 data products. Royal

Netherlands Meteorological Institute. Retrieved June 29, 2021, from

https://sentinel.esa.int/documents/247904/2476257/Sentinel-5P-TROPOMI-ATBD-

NO2-data-products

Gleason, K. L. (2008, March 20). *Science: Ozone basics*. National Oceanic and Atmospheric

Administration. Retrieved March 13, 2021, from

https://www.ozonelayer.noaa.gov/science/basics.htm

Goldberg, D. L., Vinciguerra, T. P., Anderson, D. C., Hembeck, L., Canty, T. P., Ehrman, S.

H., … Dickerson, R. R. (2016). CAMx ozone source attribution in the eastern United

States using guidance from observations during DISCOVER-AQ Maryland.

Geophysical Research Letters, 43(5), 2249-2258.

https://doi.org/10.1002/2015GL067332

Haagen-Smit, A. J. (1952). Chemistry and physiology of Los Angeles smog. *Industrial and Engineering Chemistry, 44*(6), 1342-1346. https://doi.org/10.1021/ie50510a045

Heckert, A. (2016). *Kolmogorov Smirnov two sample*. National Institute of Standards and Technology. Retrieved August 12, 2020, from https://www.itl.nist.gov/div898/software/dataplot/refman1/auxillar/ks2samp.htm

Hu, X.-M., Klein, P. M., & Xue, M. (2013). Evaluation of the updated YSU planetary boundary layer scheme within WRF for wind resource and air quality assessments. *Journal of Geophysical Research: Atmospheres, 118*(18), 10490-10505. https://doi.org/10.1002/jgrd.50823

Jacob, D. J. (1999). *Introduction to atmospheric chemistry*. Princeton University Press. Retrieved May 4, 2021, from http://acmg.seas.harvard.edu/people/faculty/djj/book/

Jacob, D. J. (2000). Heterogeneous chemistry and tropospheric ozone. *Atmospheric Environment, 34*(12-14), 2131-2159. https://doi.org/10.1016/S1352-2310(99)00462-8

Jerrett, M., Burnett, R. T., Pope III, C. A., Ito, K., Thurston, G., Krewski, D., … Thun, M. (2009). Long-term ozone exposure and mortality. *The New England Journal of Medicine, 360*(11), 1085-1095. https://doi.org/10.1056/NEJMoa0803894

Jin, X., Fiore, A., Boersma, K. F., De Smedt, I., & Valin, L. (2020). Inferring changes in summertime surface ozone−NO_x−VOC chemistry over U.S. urban areas from two decades of satellite and ground-based observations. *Environmental Science & Technology, 54*(11), 6518-6529. https://doi.org/10.1021/acs.est.9b07785

Jin, X., Fiore, A. M., Murray, L. T., Valin, L. C., Lamsal, L. N., Duncan, B., … Tonnesen, G.
S. (2017). Evaluating a space-based indicator of surface ozone-NO_x-VOC sensitivity
ver midlatitude source regions and application to decadal trends. *Journal of
Geophysical Research: Atmospheres, 122*(19), 10439-10461.
https://doi.org/10.1002/2017JD026720

Jin, X., & Holloway, T. (2015). Spatial and temporal variability of ozone sensitivity over
China observed from the Ozone Monitoring Instrument. *Journal of Geophysical
Research: Atmospheres, 120*(14), 7229-7246. https://doi.org/10.1002/2015JD023250

Kleinman, L. I., Daum, P. H., Imre, D. G., Lee, J. H., Lee, Y.-N., … Newman, L. (2000).
Ozone production in the New York City urban plume. *Journal of Geophysical
Research: Atmospheres, 105*(D11), 14495-14511.
https://doi.org/10.1029/2000JD900011

Li, X., Wang, S., Zhou, R., & Zhou, B. (2014). Urban atmospheric formaldehyde
concentrations measured by a differential optical absorption spectroscopy method.
Environmental Science: Processes Impacts, 16(2), 291-297.
https://doi.org/10.1039/c3em00545c

Martin, R. V., Fiore, A. M., & Donkelaar, A. V. (2004). Space-based diagnosis of surface
ozone sensitivity to anthropogenic emissions. *Geophysical Research Letters, 31*(6),
L06120. https://doi.org/10.1029/2004GL019416

Mazzuca, G. M., Ren, X., Loughner, C. P., Estes, M., Crawford, J. H., Pickering, K. E., …
Dickerson, R. R. (2016). Ozone production and its sensitivity to NO_x and VOCs:
results from the DISCOVER-AQ field experiment, Houston 2013. *Atmospheric

Chemistry and Physics, 16(22), 14463-14474. https://doi.org/10.5194/acp-16-14463-2016

Myneni, R. B. (2018). *VIIRS leaf area index (LAI) and fraction of photosynthetically active radiation absorbed by vegetation (FPAR) product algorithm theoretical basis document (ATBD)*. United States Geological Survey. Retrieved January 20, 2021, from https://lpdaac.usgs.gov/documents/125/VNP15_ATBD.pdf

Sillman, S. (1995). The use of NO_y, H_2O_2, and HNO_3 as indicators for ozone-NO_x-hydrocarbon sensitivity in urban locations. *Journal of Geophysical Research: Atmospheres, 100*(D7), 14175-14188. http://dx.doi.org/10.1029/94JD02953

Sillman, S., & Samson, P. J. (1995). Impact of temperature on oxidant photochemistry in urban, polluted rural and remote environments. *Journal of Geophysical Research: Atmospheres, 100*(D6), 11497-11508. https://doi.org/10.1029/94JD02146

Steltman, H. (2018). *Approximations for mean and variance of a ratio*. Carnegie Mellon University. Retrieved July 16, 2021, from https://www.stat.cmu.edu/~hseltman/files/ratio.pdf

Thompson, G., Field, P. R., Rasmussen, R. M., & Hall, W. D. (2008). Explicit forecasts of winter precipitation using an improved bulk microphysics scheme. Part II: implementation of a new snow parameterization. *Monthly Weather Review, 136*(12), 5095-5115. https://doi.org/10.1175/2008MWR2387.1

Tonnesen, G. S., & Dennis, R. L. (2000). Analysis of radical propagation efficiency to assess ozone sensitivity to hydrocarbons and NO_x 2. Long-lived species as indicators of

ozone concentration sensitivity. *Journal of Geophysical Research, 105*(D7), 9227-
9241. https://doi.org/10.1029/1999JD900372

Turner, M. C., Jerrett, M., Pope II, C. A., Krewski, D., Gapstur, S. M., Diver, W. R., …
Burnett, R. T. (2016). Long-term ozone exposure and mortality in a large prospective
study. *American Journal of Respiratory and Critical Care Medicine, 193*(10), 1134-
1142. https://doi.org/10.1164/rccm.201508-1633OC

U.S. EPA. (2020a, August 6). *Summary of the Clean Air Act*. United States Environmental
Protection Agency. Retrieved May 4, 2021, from https://www.epa.gov/laws-
regulations/summary-clean-air-act

U.S. EPA. (2021a, January 4). *Ozone national ambient air quality standards (NAAQS)*.
United States Environmental Protection Agency. Retrieved May 4, 2021, from
https://www.epa.gov/ground-level-ozone-pollution/ozone-national-ambient-air-
quality-standards-naaqs#rule-summary

U.S. EPA. (2021b, April 28). *Ground-level ozone basics*. United States Environmental
Protection Agency. Retrieved May 3, 2021, from https://www.epa.gov/ground-level-
ozone-pollution/ground-level-ozone-
basics#:~:text=Breathing%20elevated%20concentrations%20of%20ozone,leading%2
0to%20increased%20medical%20care%20

U.S. EPA. (2021c, April 30). *8-hour ozone nonattainment areas (2015 standard)*. United
States Environmental Protection Agency. Retrieved May 3, 2021, from
https://www3.epa.gov/airquality/greenbook/map8hr_2015.html

Valin, L. C., Fiore, A. M., Chance, K., & González Abad, G. (2016). The role of OH production in interpreting the variability of CH_2O columns in the southeast U.S. *Journal of Geophysical Research: Atmospheres, 121*(1), 478-493. https://doi.org/10.1002/2015JD024012

Veefkind, J. P., Aben, I., McMullan, K., Förster, H., de Vries, J., Otter, G., … Levelt, P. F. (2012). TROPOMI on the ESA Sentinel-5 Precursor: A GMES mission for global observations of the atmospheric composition for climate, air quality and ozone layer applications. *Remote Sensing of Environment, 120*, 70-83. https://doi.org/10.1016/j.rse.2011.09.027

Vermeuel, M. P., Novak, G. A., Alwe, H. D., Hughes, D. D., Kaleel, R., Dickens, A. F., … Bertram, T. H. (2019). Sensitivity of ozone production to NO_x and VOC along the Lake Michigan coastline. *Journal of Geophysical Research: Atmospheres, 124*(20), 10989-11006. https://doi.org/10.1029/2019JD030842

Wang, Z., Anthony, J. L., Erickson, L. E., Higgins, M. J., & Newmark, G. L. (2020). Nitrogen dioxide and ozone pollution in the Chicago Metropolitan Area. *Journal of Environmental Protection, 11*(8), 551-569. https://doi.org/10.4236/jep.2020.118033

Zehner, C. (n.d.). *Status of the Sentinel-5 Precursor* [Presentation Slides]. European Space Agency. Retrieved May 7, 2021, from https://ceos.org/document_management/Virtual_Constellations/ACC/Meetings/AC-VC-13/ACVC13_presentations_pdf/Day%201%20GHG/4_CEOS-AC-VC-13_GHG_Sentinel-5P_Claus_Zehner.pdf

Zoogman, P., Liu, X., Suleiman, R. M., Pennington, W. F., Flittner, D. E., Al-Saadi, J. A., …

Chance, K. (2017). Tropospheric emissions: Monitoring of pollution (TEMPO).

Journal of Quantitative Spectroscopy and Radiative Transfer, 186, 17-39.

https://doi.org/10.1016/j.jqsrt.2016.05.008

DATA CITATIONS

Conley, S. (2019). *Scientific Aviation – photochemical trace gases – LMOS 2017* [.ict files
with airborne in situ NO_2 observations]. Hampton, VA, USA, Airborne Science Data
for Atmospheric Composition, NASA Langley Research Center. Retrieved March 1,
2021, from https://www-air.larc.nasa.gov/cgi-bin/ArcView/lmos?SCI-AVIATION=1

German Aerospace Center (DLR). (2019a). *Sentinel-5P TROPOMI tropospheric
formaldehyde HCHO 1-orbit L2 7km x 3.5km* [Copernicus Sentinel data processed by
ESA]. Greenbelt, MD, USA, Goddard Earth Sciences Data and Information Services
Center (GES DISC). Retrieved March 15, 2020, from https://doi.org/10.5270/S5P-
tjlxfd2

German Aerospace Center (DLR). (2019b). *Sentinel-5P TROPOMI tropospheric
formaldehyde HCHO 1-orbit L2 5.5km x 3.5km* [Copernicus Sentinel data processed
by ESA]. Greenbelt, MD, USA, Goddard Earth Sciences Data and Information
Services Center (GES DISC). Retrieved March 15, 2020, from
https://doi.org/10.5270/S5P-tjlxfd2

Kenski, D. (2020). *Ozone episodes by NAA* [file with ozone exceedance data for NAAs
within or near the LADCO domain]. U.S. EPA data processed by D. Kenski at
LADCO. Retrieved April 1, 2020, via personal communication with D. Kenski at
LADCO.

Koninklijk Nederlands Meteorologisch Instituut (KNMI). (2018). *Sentinel-5P TROPOMI
tropospheric NO_2 1-orbit L2 7km x 3.5km* [Copernicus Sentinel data processed by

ESA]. Greenbelt, MD, USA, Goddard Earth Sciences Data and Information Services

Center (GES DISC). Retrieved March 15, 2020, from https://doi.org/10.5270/S5P-

s4ljg54

Koninklijk Nederlands Meteorologisch Instituut (KNMI). (2019). *Sentinel-5P TROPOMI*

tropospheric NO$_2$ 1-orbit L2 5.5km x 3.5km [Copernicus Sentinel data processed by

ESA]. Greenbelt, MD, USA, Goddard Earth Sciences Data and Information Services

Center (GES DISC). Retrieved March 15, 2020, from https://doi.org/10.5270/S5P-

s4ljg54

Otkin, J. [PI], Adelman, Z., Hain, C., Case, J., Harkey, M., Pierce, R. B., Heidinger, A., &

Szykman, J. (2021). *A satellite constrained meteorological modeling platform for*

LADCO states SIP development (NASA-funded project) – 1.3 km^2 CMAQ output

[netcdf files with gridded HCHO and NO$_2$ data]. Retrieved March 15, 2021, via

personal communication with R. B. Pierce.

U.S. EPA. (2020b, March 4). *AQS_sites* [.csv file with EPA PAMS site information].

Retrieved April 15, 2020, via personal communication with D. Kenski at LADCO.

U.S. EPA. (2020c, March 4). *Photochemical Assessment Monitoring Stations (PAMS) raw*

data [.txt file with HCHO and NO$_2$ data]. Retrieved April 15, 2020, via personal

communication with D. Kenski at LADCO.

U.S. EPA Office of Research and Development, National Exposure Research Laboratory.

(2017). *In-situ, gas-phase HCHO, HCOOH, and H$_2$O mixing ratios – LMOS 2017*

[.ict file with HCHO data]. Hampton, VA, USA, Airborne Science Data for

Atmospheric Composition, NASA Langley Research Center. Retrieved June 1, 2020,

from https://www-air.larc.nasa.gov/cgi-bin/ArcView/lmos?GROUND-

SHEBOYGAN=1

U.S. EPA Office of Research and Development, National Exposure Research Laboratory.

(2018). *Surface trace gas and meteorological measurements – LMOS 2017* [.ict file

with NO_2 data]. Hampton, VA, USA, Airborne Science Data for Atmospheric

Composition, NASA Langley Research Center. Retrieved June 1, 2020, from

https://www-air.larc.nasa.gov/cgi-bin/ArcView/lmos?GROUND-SHEBOYGAN=1